We are IntechOpen,
the world's leading publisher of
Open Access books
Built by scientists, for scientists

4,800
Open access books available

122,000
International authors and editors

135M
Downloads

154
Countries delivered to

Our authors are among the

TOP 1%
most cited scientists

12.2%
Contributors from top 500 universities

CLARIVATE ANALYTICS

BOOK CITATION INDEX

INDEXED

WEB OF SCIENCE™

Selection of our books indexed in the Book Citation Index
in Web of Science™ Core Collection (BKCI)

Interested in publishing with us?
Contact book.department@intechopen.com

Numbers displayed above are based on latest data collected.
For more information visit www.intechopen.com

9

Microwave-Induced Combustion Synthesis of Luminescent Aluminate Powders

A. Potdevin[1,2], N. Pradal[1,3], M.-L. François[1,3],
G. Chadeyron[1,2], D. Boyer[1,2] and R. Mahiou[1,3]
*[1]Clermont Université, Université Blaise Pascal,
Laboratoire des Matériaux Inorganiques, Clermont-Ferrand,
[2]Clermont Université, ENSCCF, Laboratoire des Matériaux Inorganiques,
Clermont-Ferrand,
[3]CNRS, UMR 6002, LMI, F-63177 Aubière,
France*

1. Introduction

Due to the current environmental directives concerning the use of hazardous mercury in lighting devices and the necessity to save global energy, new economical and eco-friendly light sources are being developed. In this context, phosphor-converted light emitting diodes (LEDs) appear as the most interesting candidates to replace energy-greedy incandescent light bulbs and fluorescent lamps. Indeed, it is now a mature technology that can compete with the former ones, especially thanks to their long lifetime, low-power consumption, high energy efficiency and robustness (Höppe 2009; Huang et al. 2009; Smet et al. 2011). However, some drawbacks remain, such as the lack of high colour rendering devices.

Until recently, white LEDs were almost only based on the association of blue GaN LED with a yellow phosphor, $Y_3Al_5O_{12}:Ce^{3+}$ (YAG:Ce). These devices are characterized by a high colour temperature due to a lack of red contribution. Another approach consists in combining (Ga,Al)N near ultraviolet (UV) pumping LEDs with red, green and blue phosphors. This gives access to a wide range of colours and controlled colour rendering. The optical performances of the LEDs-based light sources rely on the physical characteristics of the semi-conductor as well as the features of the phosphors. In particular, the luminescence properties of phosphors are known to be dependent on their morphology, their size and their crystallinity. Defects have also to be avoided because they act as luminescence shifters or quenchers. Furthermore, it has been proved in several recent studies that white LEDs using smaller particles size, with narrower grain size distribution, required a lower amount of phosphor to get similar efficiency than LEDs using bigger particles (Huang et al. 2009; Jia et al. 2007). It has been related to the reduction of internal light scattering when these nanoparticles are directly coated onto the LEDs surface at the front of this.

Based on this behaviour, it seems necessary to develop highly luminescent nanosized or nanostructured phosphors, easy to shape as luminescent films. Among the phosphors

suitable for white LEDs, we have chosen to work on YAG:Ce and $BaMgAl_{10}O_{17}:Eu^{2+}$ (BAM:Eu) for blue and UV LEDs-based devices respectively. Moreover, together with its possible application in UV-LEDs based lighting devices, BAM:Eu represents the most interesting blue phosphor for Hg-free lamps based on Xe-Ne plasma and for plasma display panels(Chen & Yan 2007; Shen et al. 2010; Smet et al. 2011).

Traditionally, these phosphors are obtained via energy-greedy solid-state reactions involving very high synthesis temperatures, associated with grinding and milling (Shionoya 1998). These synthesis routes lead to microsized particles exhibiting surface defects and a large particle size distribution, which is prejudicial to optical performances. The necessity to develop nanostructured phosphors has entailed the emergence of numerous chemical synthesis techniques for these aluminates: solvothermal, sol-gel, co-precipitation, spray pyrolysis...(Kang et al. 1998; Lee et al. 2009; Lu et al. 2006; Pan et al. 2004; Potdevin et al. 2007; Zhang et al. 2010). These methods involve a homogeneous mixing of metal ions by using precursors in solution. Next to them, the combustion process appears as an attractive alternative thanks to its simplicity and its low cost; in particular, solution combustion synthesis (SCS) methods allow to prepare various nanosized oxides of high purity, using different organic fuels (Mukasyan et al. 2007).

Recently, a new kind of SCS routes has been used for the synthesis of oxides: microwave-induced SCS (MISCS). The use of microwave in combustion synthesis presents several advantages (shortened synthesis times, enhanced reaction kinetics...) thanks to dissimilar heating mechanisms compared to the conventional combustion synthesis. For example, microwave radiations are immediately absorbed by the entire sample and interact from bulk to the surface leading to volumetric heating in contrast with conventional sintering in which heating takes place by radiation or conduction of the heat energy from the surface to the core. This process has been recently used for the preparation of various oxides as well as luminescent aluminates such as YAG:Ce and BAM:Eu (Chen et al. 2009; Fu 2006; Jung & Kang 2010).

In this chapter, we report the elaboration of undoped and Ce^{3+}-doped YAG powders as well as BAM:Eu ones by MISCS. Different amounts of urea, employed as fuel, were used and a comparative investigation has been carried out on phosphors properties regarding this content. Structural, morphological and optical features of powders have been studied by means of X-ray diffraction (XRD), infrared (IR) spectroscopy, scanning and transmission electron microscopies (TEM/SEM) and photoluminescence. Morphological and optical properties have also been compared with those of commercial phosphors.

2. Experimental section

2.1 Synthesis procedures

The two synthesis procedures used for YAG and BAM phases were very close to each other. They are based on the works of Y.-P. Fu and Z. Chen *et al.*, respectively (Chen et al. 2009; Fu 2006). For sake of clarity, the differences between the two procedures will be detailed in the following paragraphs.

For both processes, employed precursors are metal nitrates and urea, used as oxidizers and fuel, respectively. Metal nitrates were weighed stoichiometrically, dissolved in distilled water

in a beaker and stirred in order to obtain a clear solution. Then, urea was added with different fuel to oxidizer molar ratios (f/o). The theoretical (stoichiometric) molar ratio of urea to nitrate $(f/o)_{th}$ was determined for each process, based on the total oxidizing and reducing valencies of the oxidizer and the fuel (Jain et al. 1981). Then, the solution was either poured into a porcelain crucible or maintained in the beaker and placed into a domestic microwave oven always operating at its maximum power setting (900 W). The solution boiled, underwent a dehydration followed by nitrates and urea decomposition, leading to the formation of a large amount of gases (N_2, CO_2 and H_2O). Then, the medium reached the point of spontaneous combustion and ignited with significant swelling. The whole process, very exothermic, lasted a few minutes and resulted into foamy and friable powders.

2.1.1 $Y_3Al_5O_{12}$ and $Y_3Al_5O_{12}$:Ce^{3+}

$Y_3Al_5O_{12}$ and $Y_{2.97}Ce_{0.03}Al_5O_{12}$ powders were prepared by MISCS using $CO(NH_2)_2$ (Prolabo, purity 99.5%) as fuel and $Y(NO_3)_3 \cdot 6H_2O$ (Sigma-Aldrich, purity 99.9%), $Al(NO_3)_3 \cdot 9H_2O$ (Sigma-Aldrich, purity 99.997%) and $Ce(NO_3)_3 \cdot 5H_2O$ (Sigma-Aldrich, purity 99,9%) as metallic precursors. The $(f/o)_{th}$ in this case was determined to be 2.55/1 from the following equation (Fu 2006):

$$3Y(NO_3)_3 + 5Al(NO_3)_3 + 20CO(NH_2)_2 \rightarrow Y_3Al_5O_{12}+20CO_2+40H_2O+32N_2 \qquad (1)$$
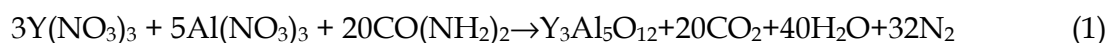
The optimal quantity of fuel has been optimized from the undoped matrix by investigating four molar ratios (f/o) [$(f/o)_{th}$, $2(f/o)_{th}$ $2.5(f/o)_{th}$ and $3(f/o)_{th}$], using the same batch of nitrate solution, divided into four beakers. Depending on the urea amount, the synthesis does not present the same characteristics. Thus, when $(f/o)=(f/o)_{th}$, no flame was observed during the microwave induced heating and the obtained powder is white. For the other molar ratios, an orangey flame is produced, as shown in Fig. 1. The obtained powders are characterized by a grey colour (mixture of grey and white powders for $2(f/o)_{th}$) (for undoped YAG).
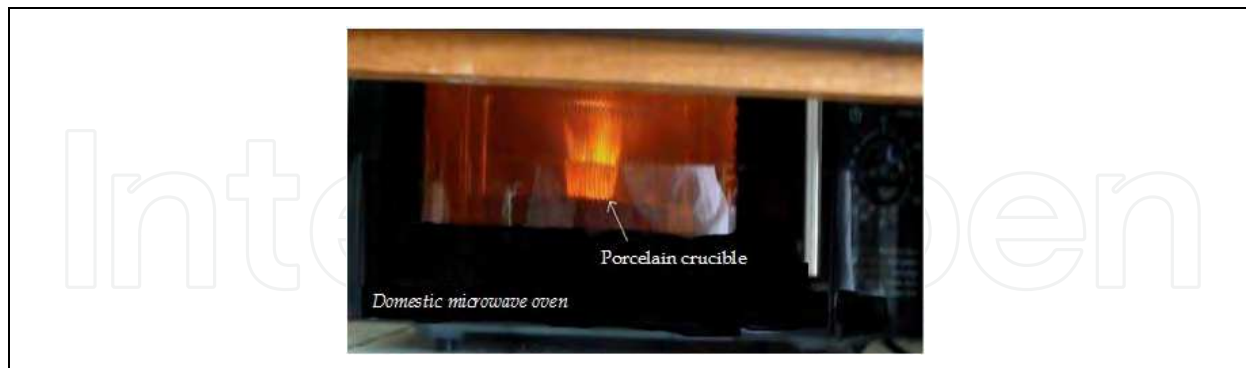

Fig. 1. Picture of a porcelain crucible containing nitrates/urea solution, ignited after few minutes of microwave irradiation.

Thanks to the XRD patterns of undoped YAG (detailed subsequently in this chapter), the amount of urea used to prepare YAG:Ce powder wad fixed to $3(f/o)_{th}$. The powder issued from this process presents a grey and a white part. When exposed to UV radiation (λ_{exc}=365 nm), only the grey part exhibits a yellow fluorescence, characteristic of Ce^{3+} ions embedded in the YAG matrix (see Fig. 2).
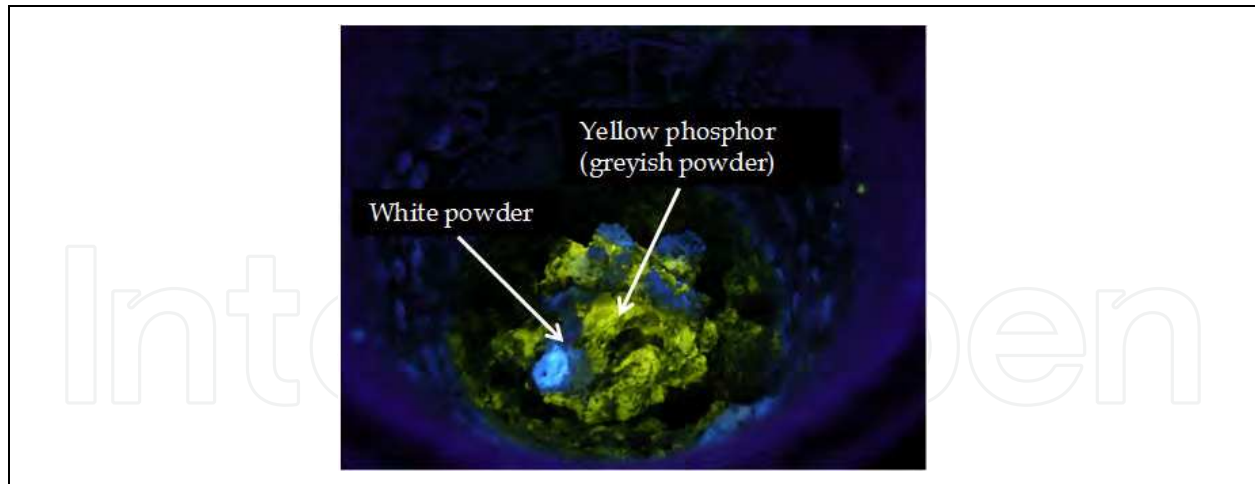
Fig. 2. Picture of as-synthesized YAG:Ce powder upon excitation at 365nm for $3(f/o)_{th}$.

This grey colour is usually characteristic of organic residues. Unfortunately, these organic residues are generally a nuisance for the optical properties since they usually act as quenching sites and result in a strong decrease of the luminescence intensity. Consequently, the YAG:Ce powder was submitted to either an acid washing or a post-calcination in air. The wash does not provoke any modification of the powder but a calcination stage of two hours at 1000°C allows obtaining a yellow powder as evidenced in the Fig. 3.

Fig. 3. Picture of as-synthesized YAG:Ce powder before(a) and after(b) post-calcination at 1000°C for 2 hours.

Hence, optical performances were assessed for the two YAG:Ce powders as well as their structural and morphological properties, in order to evidence the influence of the post-heating treatment.

2.1.2 BaMgAl$_{10}$O$_{17}$:Eu^{2+}

$Ba_{0.9}Eu_{0.1}MgAl_{10}O_{17}$ powders were prepared by MISCS using $CO(NH_2)_2$ (Prolabo, purity 99.5%) as fuel and $Ba(NO_3)_2$ (Sigma-Aldrich, purity 99+%), $Mg(NO_3)_2 \cdot 6H_2O$ (Acros organics, purity 99+%), $Al(NO_3)_3 \cdot 9H_2O$ (Sigma-Aldrich, purity 99.997%) and $Eu(NO_3)_3 \cdot 5H_2O$ (Sigma-

Aldrich, purity 99.9%) as metallic precursors. The $(f/o)_{th}$ is in this case 2.36/1. Two molar ratios were investigated: $(f/o)_{th}$ and $3(f/o)_{th}$. Contrary to the YAG synthesis, the combustion is characterized by a white flame and obtained powders are white and, when exposed to UV radiation (λ_{exc}=254 nm), they are composed of blue and red parts, as shown in Fig. 4.
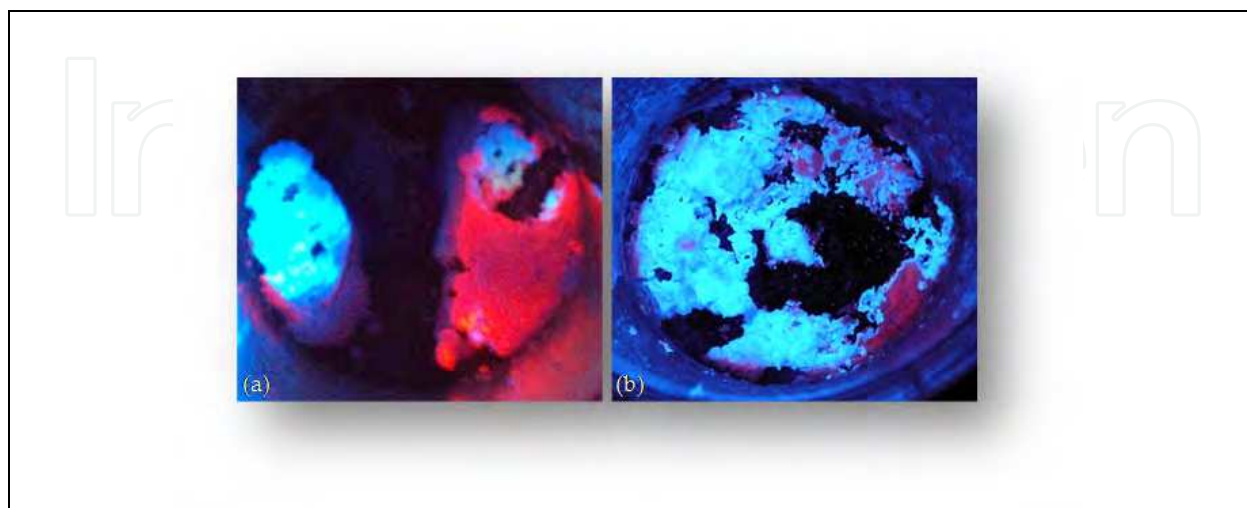

Fig. 4. Pictures of as-synthesized powders upon excitation at 254nm for (a) $(f/o)_{th}$ and (b) $3(f/o)_{th}$.

Since the part intended as phosphors for lighting devices is the blue one, this latter has been isolated before being characterized. This as-synthesized blue part contains a little fraction of $BaAl_2O_4$ (as seen later in the XRD study), consequently an additional washing step has been carried out to purify BAM phase and theoretically improve its optical performances. Thus, this powder emitting in the blue range was washed several times with acidic distilled water before being themselves characterized.

2.2 Characterization techniques

XRD patterns concerning undoped YAG and YAG:Ce phases were performed on a Siemens D500 and a Siemens D5000 diffractometers, respectively, whereas those of BAM:Eu were recorded on a Philips Xpert Pro diffractometer. All the diffractometers operated with the Cu-Kα radiation (λ=1,5406Å). CaRIne Crystallography v3.1 software was used to simulate XRD pattern of BAM from the crystallographic data (Kim et al. 2002). An attenuated total reflection (ATR) accessory installed on a Nicolet FTIR spectrometer was used to record ATR spectra for all powders.

Micrographs were mainly recorded by means of a ZEISS Supra 55VP scanning electron microscope operating in high vacuum between 3 and 5 kV using secondary electron detector (Everhart-Thornley detector). Specimens were prepared by sticking powder onto the surface of an adhesive carbon film. BAM powders morphology was also investigated by means of a transmission electron microscope (Hitachi H7650 120kV) using a 80 kV acceleration voltage and combined with a Hamamatsu AMT HR 1Kx1K CCD camera placed in a side position. Samples were coated into a resin, cut with a microtome and then placed in the microscope.

Emission and excitation spectra of BAM:Eu powders were performed on a Jobin-Yvon set-up consisting of a Xe lamp operating at 400 W and two monochromators (Triax 550 and Triax 180) combined with a cryogenically cooled charge-coupled device (CCD) camera (Jobin-Yvon Symphony LN2 series) for emission spectra and with a Hamamatsu 980 photomultiplicator for excitation ones. Emission and excitation features of YAG:Ce powders as well as absolute photo-luminescence quantum yields values of all powders were measured using C9920-02G PL-QY measurement system from Hamamatsu. The setup comprises a 150W monochromatized Xe lamp, an integrating sphere (Spectralon Coating, $\emptyset$ = 3.3 inch) and a high sensitivity CCD spectrometer for detecting the whole spectral luminescence. The automatically controlled excitation wavelength range spread from 250 nm to 950 nm with a resolution bandwidth better than 5 nm. This device was also employed to determine the trichromatic coordinates of BAM powders. Thanks to the software Color Calculator from Radiant Imaging, these coordinates have been placed in the CIE colour diagram. These data allow assessing if the obtained phosphors are suitable for replacing commercial phosphors in lighting devices. It must be specified that all luminescence performances have been recorded at room temperature.

3. A yellow phosphor: $Y_3Al_5O_{12}$:Ce^{3+}

3.1 Structural properties

Structural properties of undoped YAG and YAG:Ce powders have been analysed by means of XRD and IR spectroscopy.

3.1.1 Optimization of the urea quantity from undoped YAG powders

First, the influence of the amount of urea, used as fuel, on the crystallization of the YAG phase was scrutinized. The corresponding XRD patterns are gathered in the Fig. 5.

The pattern corresponding to $(f/o)_{th}$ (Fig. 5a) is characteristic of an amorphous phase with no discernable diffraction peak. This can be explained by the fact that no flame was observed during this synthesis; hence, no combustion occurs and the temperature of the medium did not reach a sufficient value to entail any crystallization. For $2(f/o)_{th}$ (Fig. 5b), for which a flame has occurred during the synthesis, XRD pattern is characterized by diffraction peaks mainly ascribable to the YAG structure (JCPDS-file 33-0040) but several weak peaks, labeled ◆, are assigned to the intermediate hexagonal $YAlO_3$ (YAH) phase. When the quantity of urea increases, this phase progressively disappears and, for $3(f/o)_{th}$ (Fig. 5d), only pure YAG phase is obtained, with a good crystallinity. This can be explained on the basis of the thermodynamics of the combustion reaction, investigated by Mukasyan *et al.* (Mukasyan et al. 2007): the maximum combustion temperature (T_{max}) following the ignition is greatly dependent on the fuel amount. It can be assumed that the increase in (f/o) leads to the rise of T_{max}, which entails a better crystallinity and the absence of the YAH phase (directly converted into YAG phase) when (f/o) reaches $3(f/o)_{th}$.

The ATR spectra recorded for the same samples are gathered in Fig. 6. The wavenumber domain has been limited to 2000-400 cm^{-1} because this region allows observing at once vibrations relative to M-O bonds and those associated to the organic groups. As it could be expected, the sample synthesized with a quantity of urea corresponding to $(f/o)_{th}$ (Fig. 6a) is characterized by a broad IR signal below 800 cm^{-1}, ascribed to M-O bonds in an amorphous

sample, together with several bands lying from 1600 to 900 cm^{-1} related to organic precursors; indeed, as evidenced in Fig. 7, the vibration bands of the amorphous powder mainly correspond to a mixture of nitrates and urea. The shift and differences observed for these bands between the heated powder (Fig. 7A) and precursors (Fig. 7B and 7C) can be due to the fact that these latters have not undergone a microwave heating-treatment.
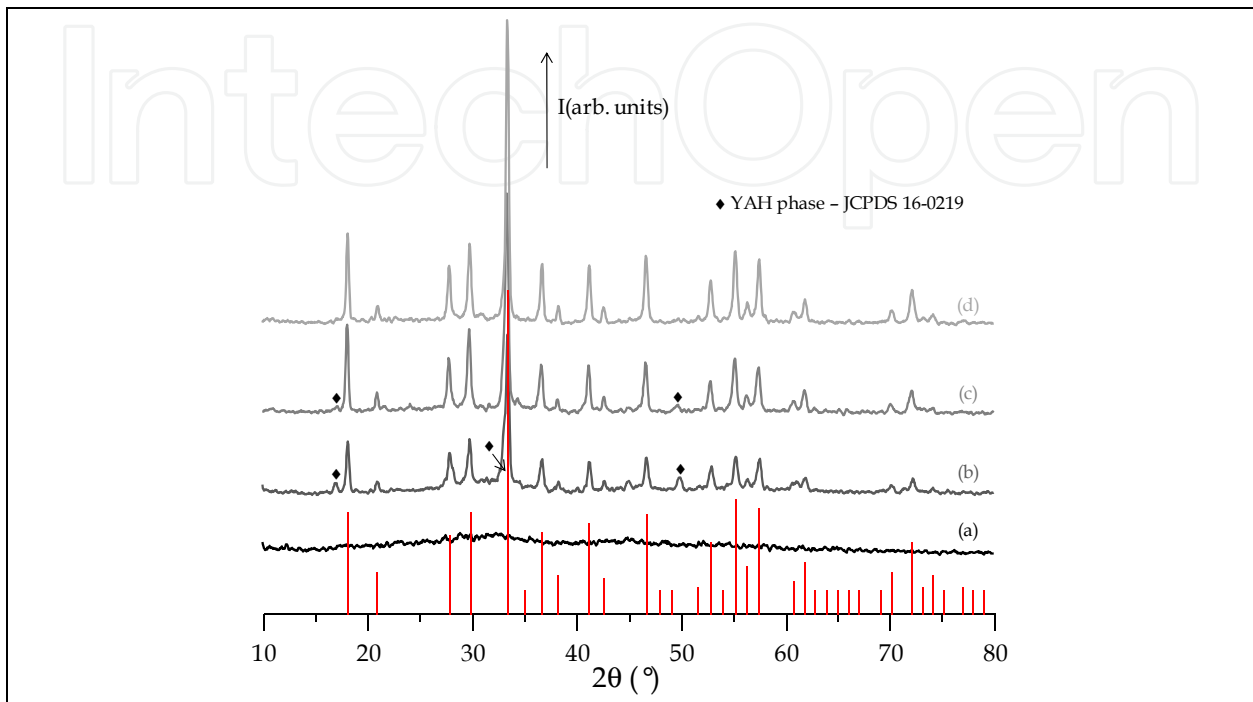

Fig. 5. XRD patterns of undoped YAG powders synthesized with (a) $(f/o)_{th}$, (b) $2(f/o)_{th}$, (c) $2.5(f/o)_{th}$ and (d) $3(f/o)_{th}$, compared to the JCPDS file 33-0040 of YAG.
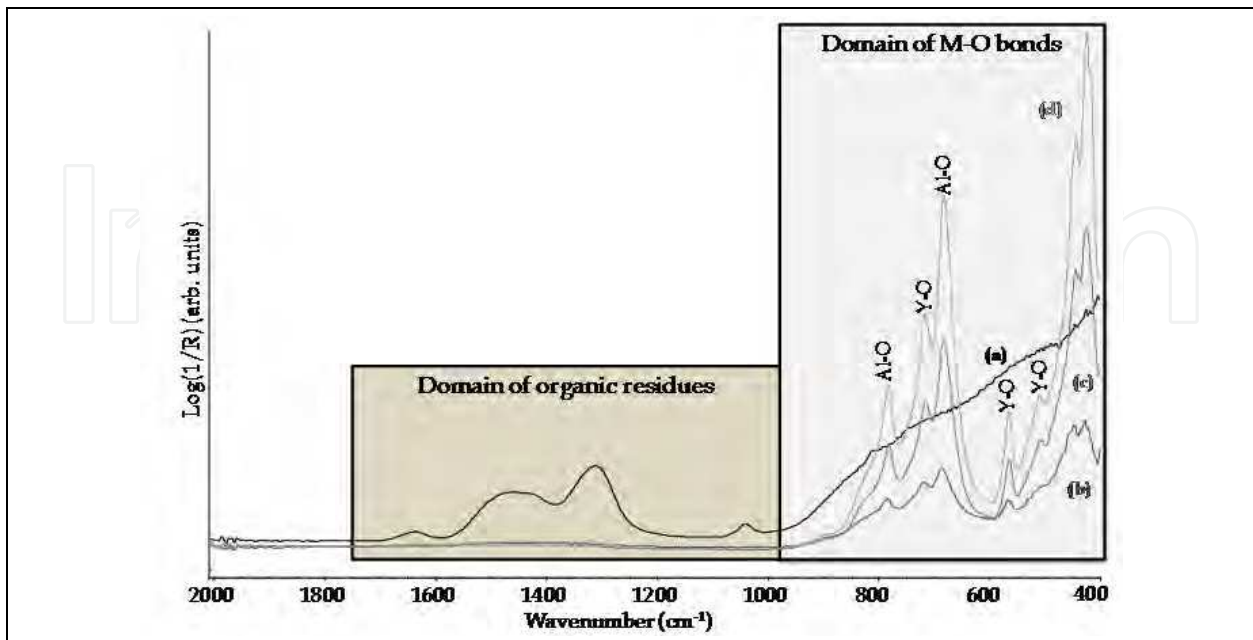
Fig. 6. ATR spectra of undoped YAG powders synthesized with (a) $(f/o)_{th}$, (b) $2(f/o)_{th}$, (c) $2.5(f/o)_{th}$ and (d) $3(f/o)_{th}$.
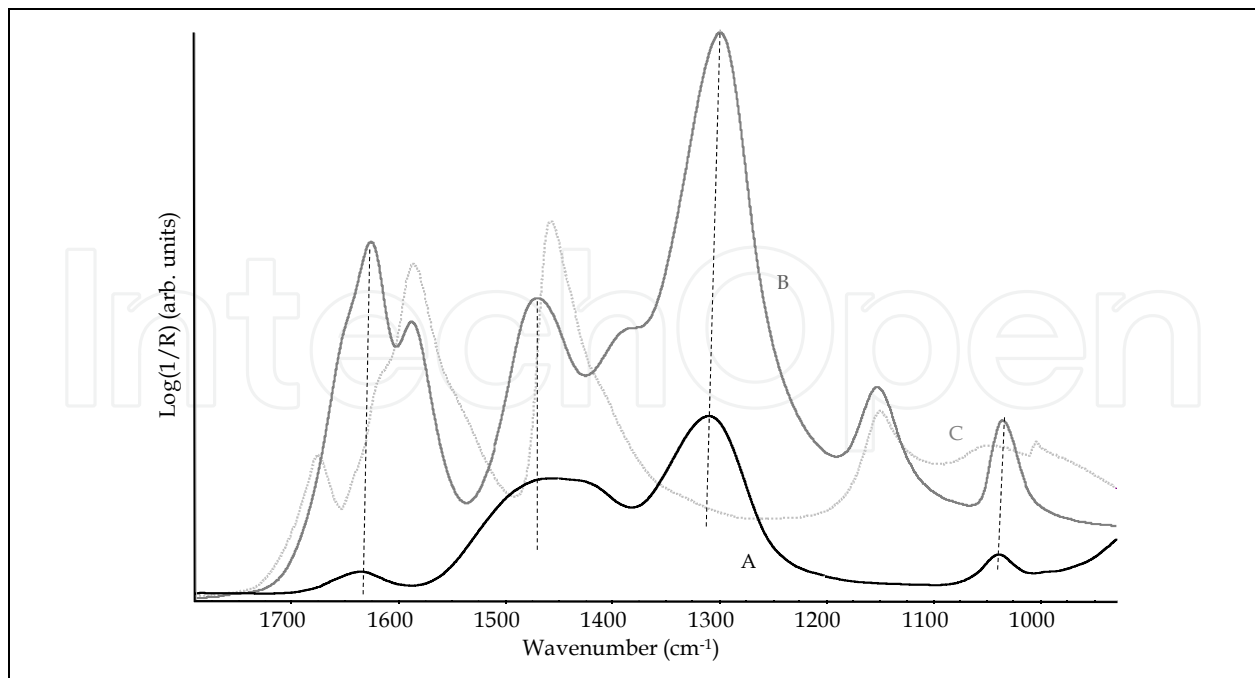
Fig. 7. ATR spectrum of undoped YAG powders synthesized with (a) $(f/o)_{th}$ compared to those of (b)yttrium nitrate and (c)urea.

When (f/o) increases, the intensity of the vibration bands between 1600 and 900 cm^{-1} significantly diminishes and these bands become negligible (Fig. 6b to 6d). The greyish colour of the powder then suggests only the presence of disordered carbonaceous impurities, in all probability resulting from the urea pyrolysis (Guo et al. 2010). Besides, when $(f/o) \geq 2(f/o)_{th}$, several vibration bands appear between 800 and 400 cm^{-1}. They are relative to Y-O and Al-O bonds in the YAG matrix and testifies that the crystallization has occurred (Hofmeister & Campbell 1992; Potdevin et al. 2010).

3.1.2 Structural analysis of YAG:Ce powders

Considering the XRD patterns obtained for the undoped YAG, the optimal ratio (f/o), leading to pure YAG phase with a good crystallinity, corresponds to $3(f/o)_{th}$ (see Fig. 5). As a consequence, Ce^{3+}-doped YAG powders have been elaborated with $3(f/o)_{th}$. As mentioned in the experimental section, the powder obtained was greyish, which is mainly related to the presence of graphite. In order to improve the optical performances of the elaborated phosphors, this carbon has to be removed from the samples. Thus, the as-prepared YAG:Ce powder was calcined at 1000°C for 2 hours. Fig. 8 represents XRD patterns of the YAG:Ce powder before and after this post-calcination step.

As-prepared YAG:Ce powder (Fig. 8a) is mainly constituted of YAG and YAlO$_3$ phases; both orthorhombic (YAP) and hexagonal (YAH) YAlO$_3$ phases coexist with YAG. After sintering at 1000°C (Fig. 8b), the YAH phase have totally been converted into YAG whereas YAP phase is still present. This behaviour can appear as surprising when compared to undoped YAG (Fig. 5) but can be explained by the difference between Y^{3+} and Ce^{3+} ionic radii. ($r_{Y^{3+}}=1.02$ Å and $r_{Ce^{3+}}=1.14$ Å in coordination VIII) (Shannon 1976). Since Ce^{3+} ions are significantly bigger, their substitution to the Y^{3+} can easily lead to the formation of

supplementary phases. The presence of YAP phase has obviously to be avoided but the powder obtained after post-calcination presents remarkable yellow luminescence upon UV and blue excitations as it will be detailed in the paragraph 3.3. The crystallinity of the post-heated powder does not seem better than that of the as-prepared one, since the diffraction intensity and the signal-to-noise ratio remain similar.
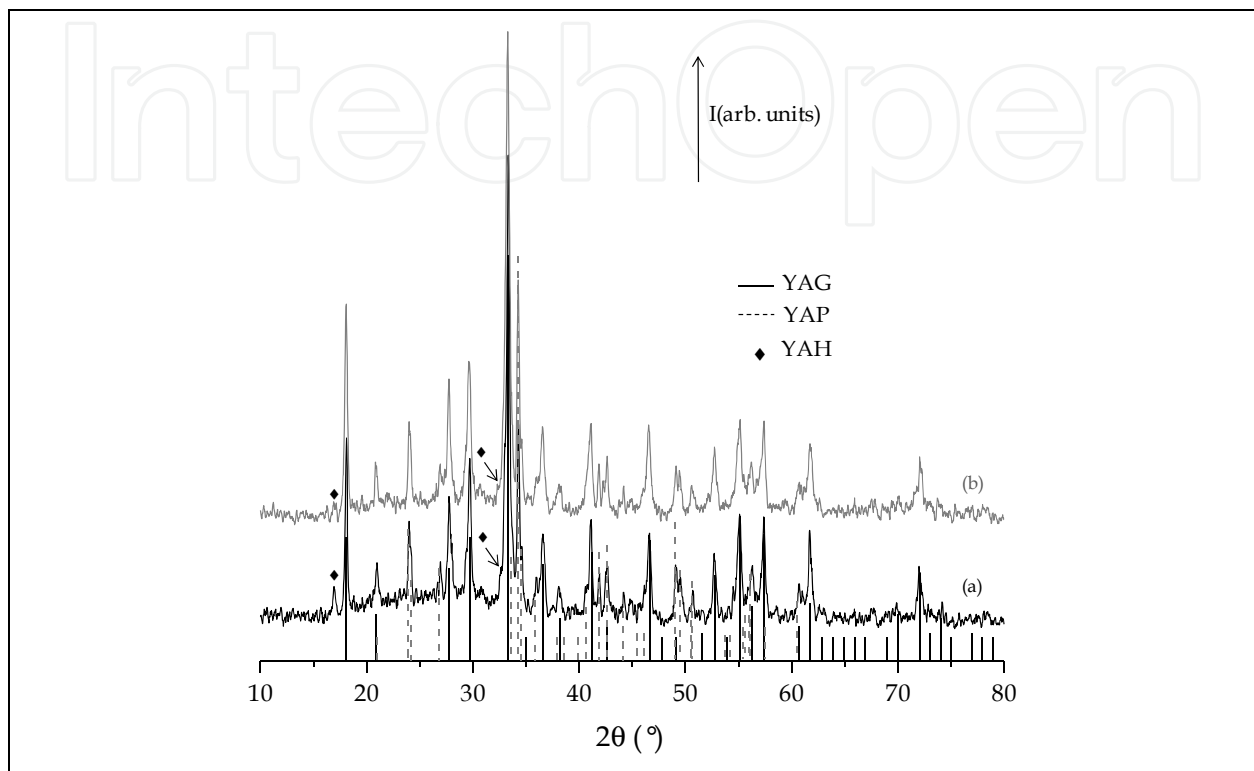

Fig. 8. XRD patterns of YAG:Ce powder synthesized with $3(f/o)_{th}$ (a)before and (b) after a post-heating treatment at 1000°C for 2 hours, compared to the JCPDS files of YAG (33-0040) and YAP (33-0041).

By modifying some synthesis parameters such as the nature of the fuel and its quantity, as well as the amount of water involved in the solution combustion synthesis, it should be possible to improve the phase purity (Mukasyan et al. 2007). The study presented in this chapter consists in a preliminary investigation, intended for evidencing the possibility to synthesize efficient phosphors by a simple and cheap method. A detailed investigation concerning the synthesis parameters of YAG:Ce powders by MISCS has not yet been carried out.

The influence of the heating-treatment at 1000°C on the structural properties of YAG:Ce powder has also been studied by IR spectroscopy. The ATR spectra presented in Fig. 9 confirm the presence of the characteristic Al-O and Y-O bonds of the YAG matrix (Hofmeister & Campbell 1992). Besides, it can be noticed that the domain of organic residues does not exhibit any specific vibration band. Only slight differences are observed between the two kinds of powders. However, the change in colour observed in Fig.3 denotes the removal of carbonaceous impurities, which has already been proved to be an important factor influencing the optical properties (Potdevin et al. 2010).
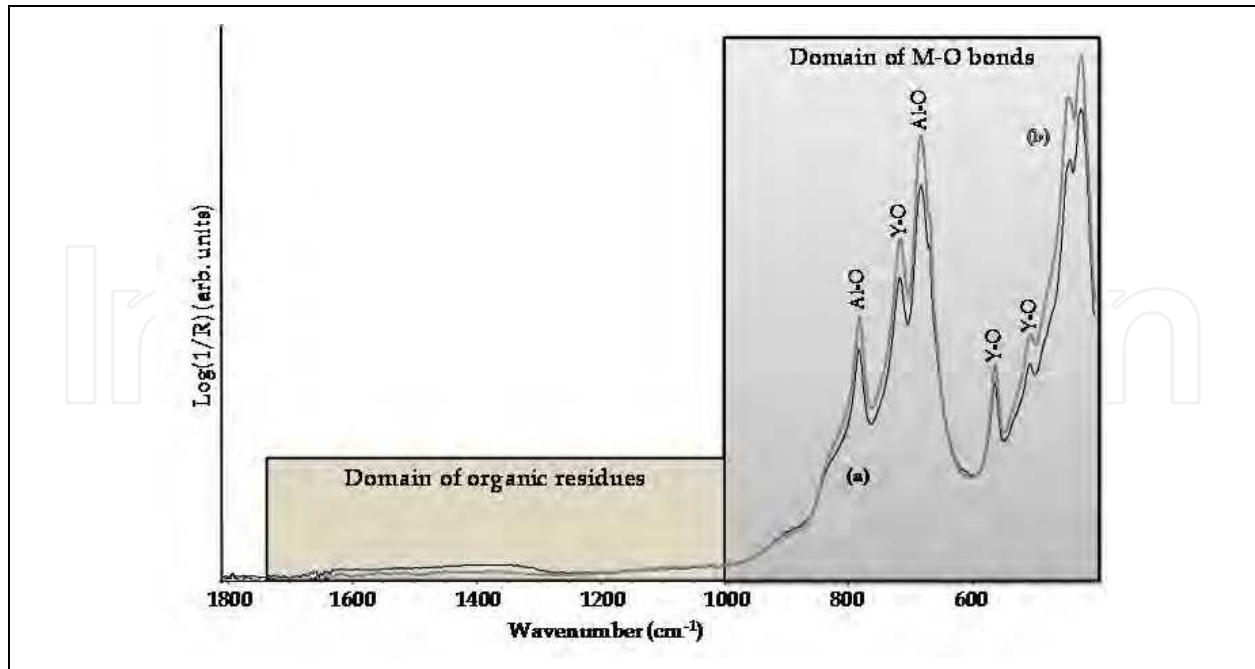
Fig. 9. ATR spectra of YAG:Ce powder synthesized with $3(f/o)_{th}$ (a)before and (b) after a post-heating treatment at 1000°C for 2 hours.

3.2 Morphological study

Micrographs corresponding to undoped YAG powders synthesized with the different amounts of urea are gathered in Fig. 10 and Fig. 11.

The pictures corresponding to the non-ignited powder (Fig. 10a and 10b) reveal dense micro-sized particles of irregular shape and very smooth surface. If compared with the sample synthesized with $(f/o)=2(f/o)_{th}$ (Fig. 10c), it can be seen that combustion reaction gives rise to a nanoporosity, correlated to the large amount of emitted gases during the ignition.
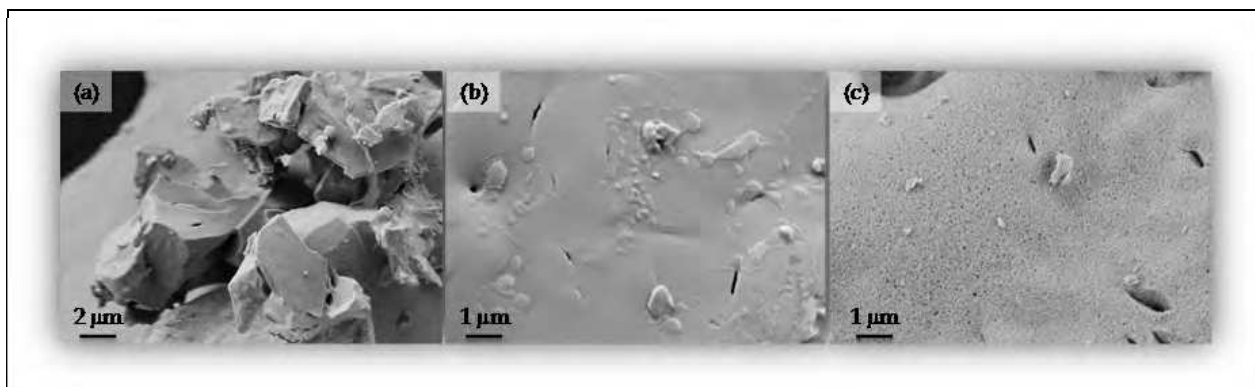
Fig. 10. SEM images of undoped YAG powders synthesized with (a,b) $(f/o)_{th}$ and (c) $2(f/o)_{th}$.

Fig. 11 exhibits SEM images of the particles elaborated with $2(f/o)_{th}$ (Fig. 11a and 11c) and $3(f/o)_{th}$ (Fig. 11b and 11d) : highly agglomerated particles with rough surface are obtained for all specimens. Nevertheless, an increase in the fuel amount entails a decrease in

agglomerates size. This can be related to the augmentation of the pressure due to extended volume of emitted gases, which gives rise to the break of interconnected structures. At higher magnifications (Fig. 11c and 11d), voids and nanopores can be well observed; they are due to the explosive character of the ignition and to the homogeneous emission of gases during the combustion, respectively.
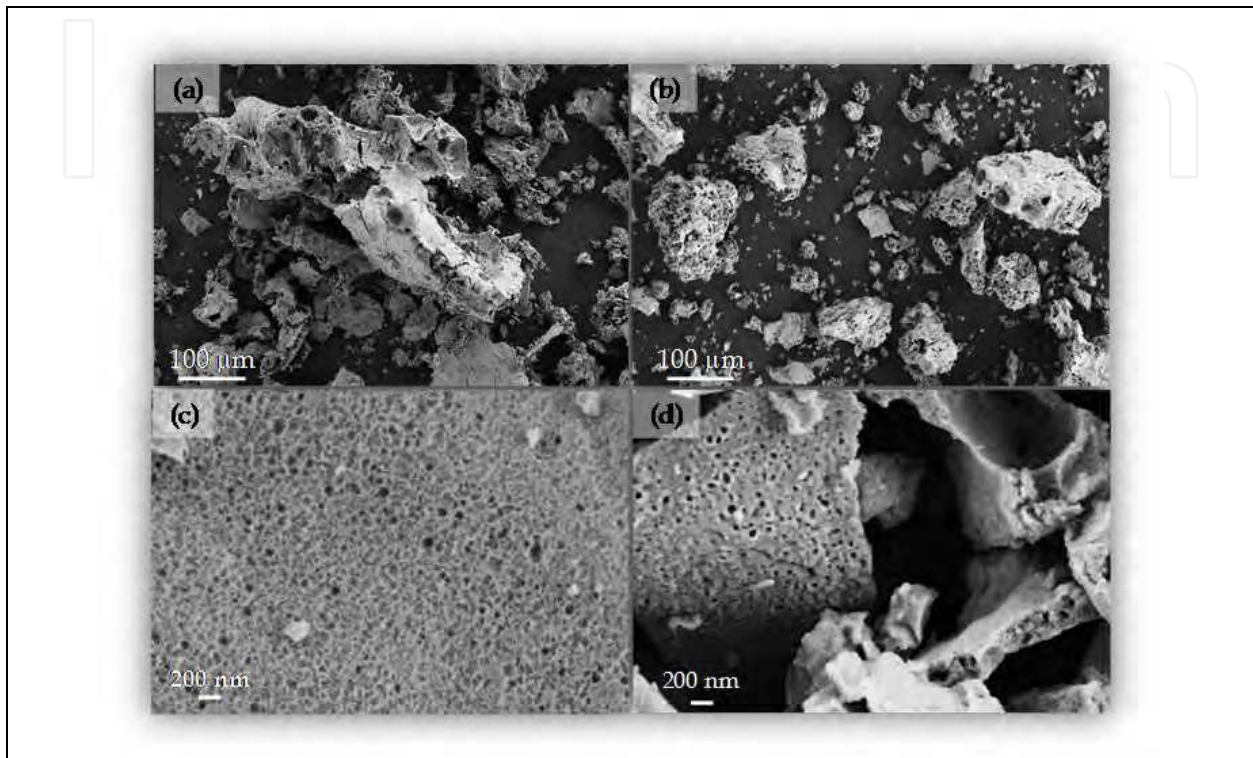

Fig. 11. SEM images of undoped YAG powders synthesized with (a,c) $2(f/o)_{th}$ and (b,d) $3(f/o)_{th}$.

The morphology of the as-synthesized YAG:Ce powder was studied by SEM and correlated to that obtained for the sintered one at 1000°C. Corresponding micrographs are presented in Fig. 12. The as-prepared YAG:Ce powder (Fig. 12a to 12c) is characterized by the same morphology than undoped YAG. No specific shape was observed. Only a highly friable powder, exhibiting large voids and nanoporosity is achieved. After the post-calcination (Fig. 12d), voids and pores remain and similar morphology is obtained. No densification has occurred which is a key point in order to use these phosphors to elaborate films. Indeed, these porous powders can be easily grinded to attain fine particles suitable for aqueous dispersions. These suspensions can then be used to prepare thick or thin luminescent films, as mentioned for BAM:Eu phosphors at the end of this chapter.

This morphology can be tailored by using different fuels, such as glycine, citric acid or carbohydrazide (Mangalaraja et al. 2009).

For comparison, SEM micrographs have been recorded from a commercial YAG:Ce powder (Phosphor Tech QMK58/F-U1). This phosphor has probably been obtained by solid-state reaction, after several hours of sintering at a temperature higher than 1300°C. As a result and as shown in Fig. 13, this phosphor is characterized by highly crystalline and well

facetted micro-sized particles. These particles are very dense and a large size distribution is highlighted. This kind of powder cannot be reasonably dispersed in a suspension in order to design homogeneous luminescent films.
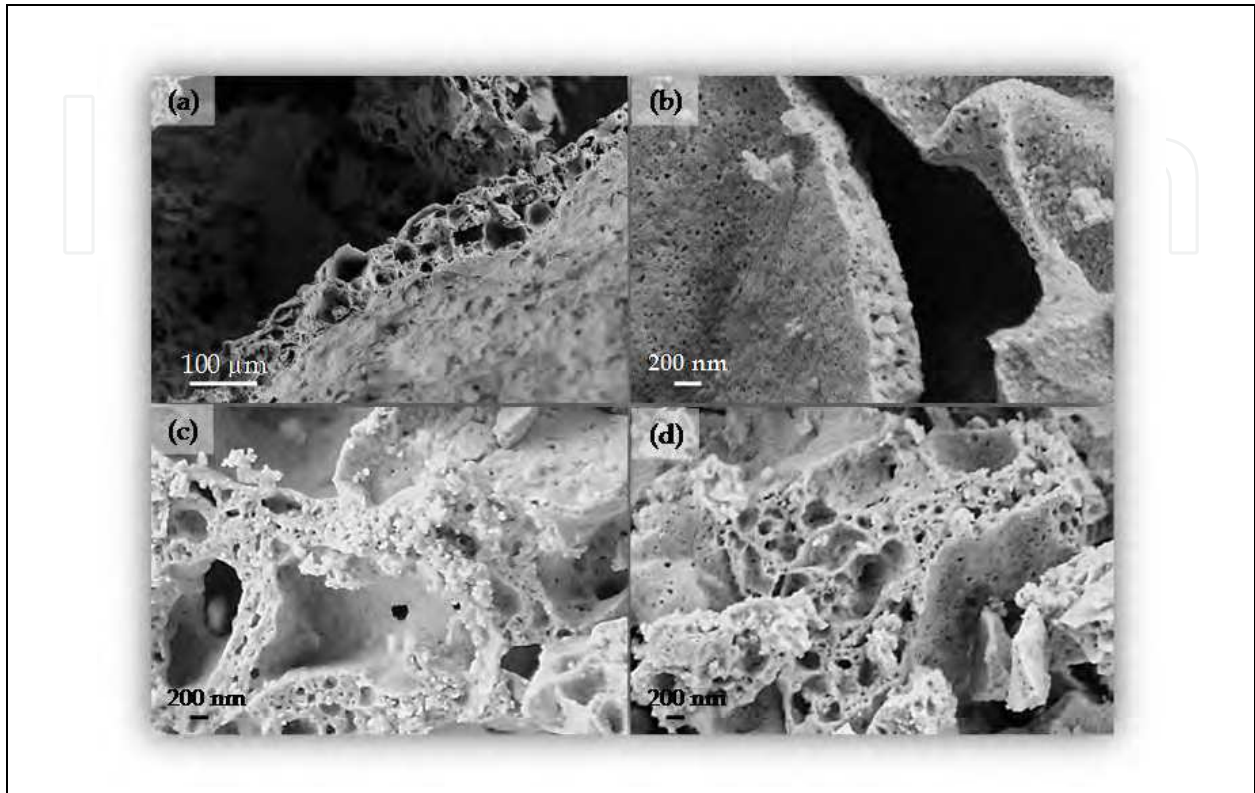

Fig. 12. SEM images of YAG:Ce powder synthesized with $3(f/o)_{th}$ (a,b,c)before and (d) after a post-heating treatment at 1000°C for 2 hours.
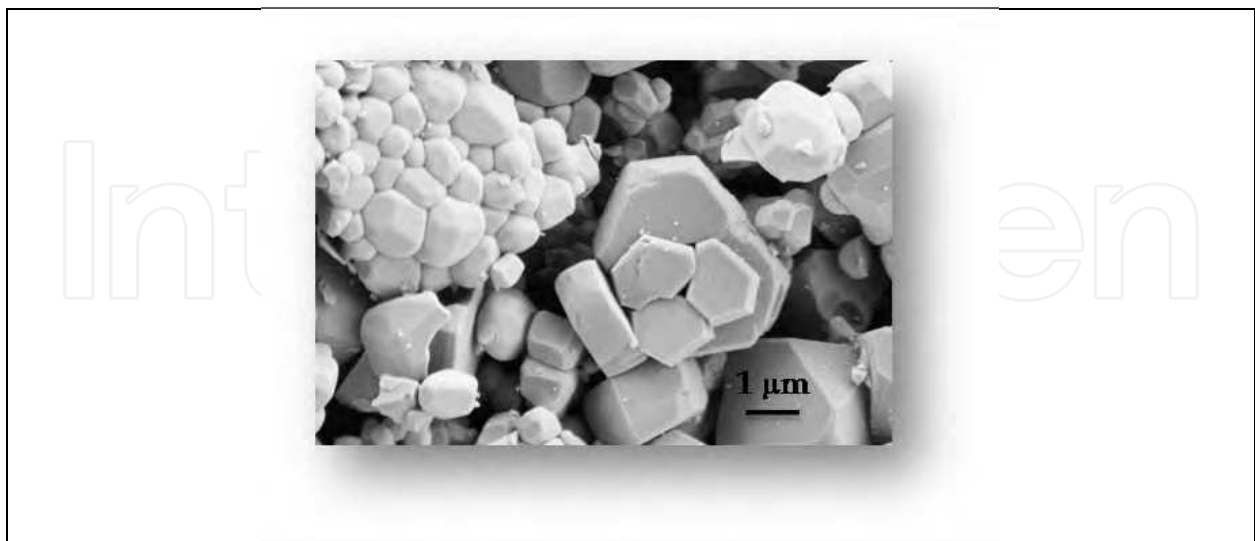

Fig. 13. SEM image of a commercial YAG:Ce powder (Phosphor Tech QMK58/F-U1.).

Furthermore, as discussed in the introduction, a large particle size distribution is generally prejudicial to the efficiency of LED-based lighting devices (Huang et al. 2009).

3.3 Photoluminescence features

Excitation spectrum obtained for post-calcined YAG:Ce powders are presented in Fig. 14. Two main excitation bands centred at 342 nm and 460 nm are observed. These excitation bands are due to the electron transitions from the ground-state $^2F_{5/2}$ of Ce^{3+} ions to the different crystal field splitting components of their 5d excited state (Blasse & Grabmaier 1994).
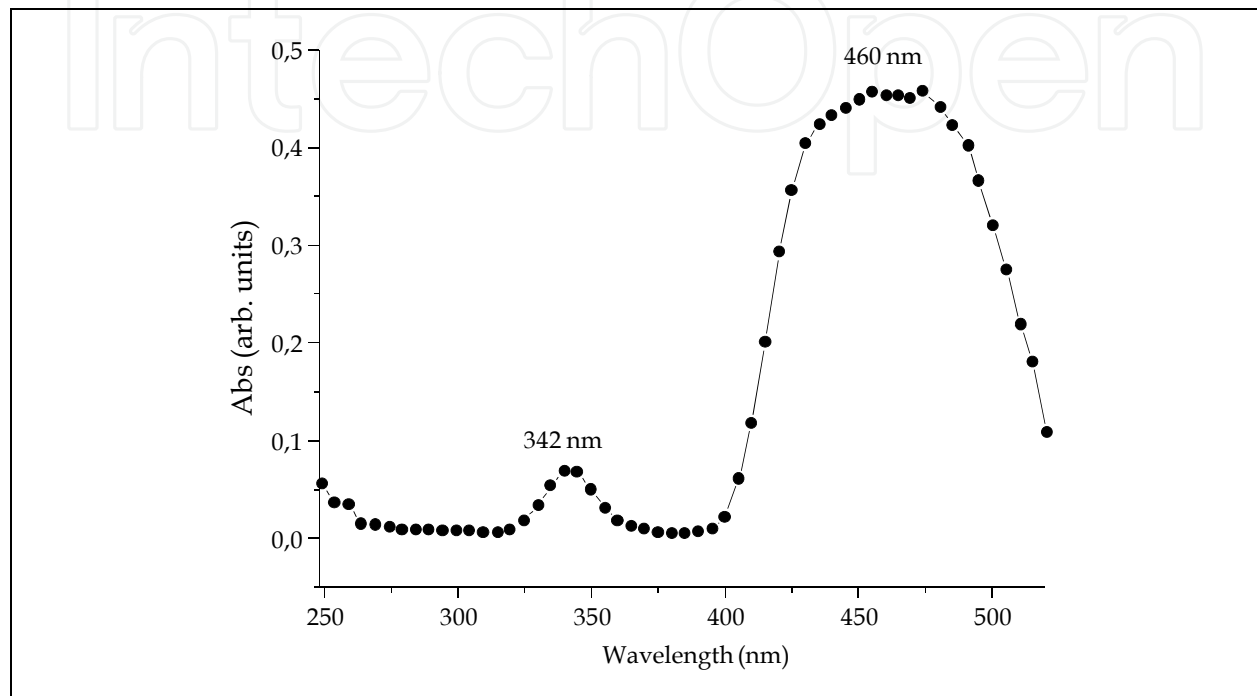

Fig. 14. Room-temperature excitation spectrum of YAG:Ce powder synthesized with $3(f/o)_{th}$ after a post-heating treatment at 1000°C for 2 hours.

The stronger band located at 460 nm matches very well the blue emission of GaN-based LED. Consequently, crystallized YAG:Ce^{3+} powders can absorb efficiently the blue emission of GaN-based LED and convert it efficiently into visible light at longer wavelength range.

Fig. 15 shows the emission spectra of YAG:Ce (1 mol%) powders before and after sintering at 1000°C recorded upon a 460 nm excitation, corresponding to a GaN-based LED. They both consist of a broad emission band due to the overlapped emission transitions relative to Ce^{3+} $^2D_{3/2}$-^7F_J transitions. For the two powders, the maximum emission intensity corresponds to a 540 nm wavelength, which is a yellowish green fluorescence. This specific feature for Ce^{3+} emission is related to strong crystal-field effects in the garnet structure (Blasse & Grabmaier 1994).

When the powder has been further calcined (Fig. 15b) the emission intensity is much more important but no red shifting is observed. Since the 5d orbit is strongly influenced by the strength and symmetry of crystal-field undergone by the Ce^{3+} ions, this testifies that the post-calcination has not entailed any crystal-field modification(Blasse & Grabmaier 1994).

Upon UV-radiation, yellow-green radiation is also observed with a significant enhancement after post-heating treatment, as evidenced in the Fig. 16.
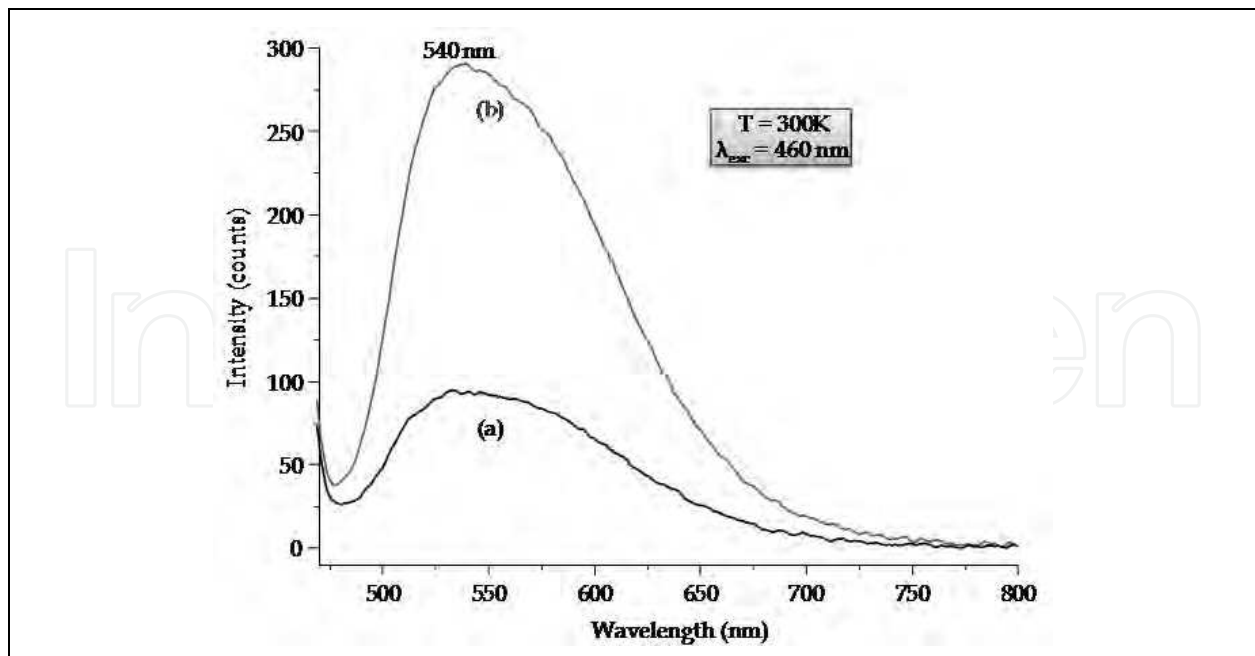
Fig. 15. Room-temperature emission spectra of YAG:Ce powder synthesized with $3(f/o)_{th}$ (a) before and (b) after a post-heating treatment at 1000°C for 2 hours.
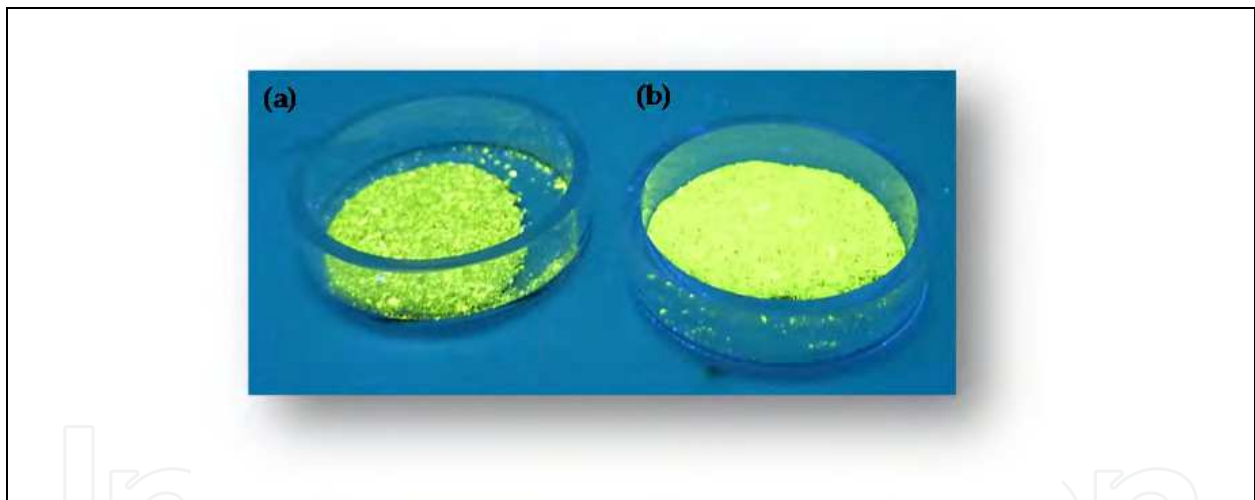

Fig. 16. Picture of as-synthesized YAG:Ce powder before(a) and after(b) post-calcination at 1000°C for 2 hours upon a 365 nm-excitation.

Finally, photoluminescence quantum yields of these YAG:Ce powders have been determined, in the range 475-800 nm, upon a 460 nm excitation, corresponding to the emission wavelength of commercialized blue LEDs. Results are gathered in Table 1.

As foreseen according to the Fig. 15, the post-heating treatment leads to a significant enhancement of the QY of the MISCS-derived YAG:Ce powder to reach 50%. This efficiency concerns a phosphor for which the synthesis parameters have not been optimized. It is better than values obtained from other combustion processes (Purwanto et al. 2008) and becomes relevant to consider the use of these phosphors in lighting devices. The QY of the commercial phosphor is obviously largely superior particularly due to its high crystallinity

(very intense diffraction peaks – results not shown). But, thanks to the features detailed before, the YAG phosphors emanating from MISCS are very promising candidates for lighting devices.

	QY(%)
Commercial	87
Before post-calcination	15
After post-calcination	50

Table 1. Absolute quantum yields (QY) for commercial and MISCS-derived YAG:Ce^{3+} powders for $3(f/o)_{th}$.

The second part of this chapter will deal with the meticulous characterization of the blue phosphor $BaMgAl_{10}O_{17}$:Eu^{2+} (BAM:Eu) obtained by MISCS.

4. A blue phosphor: $BaMgAl_{10}O_{17}$:Eu^{2+}

As seen in Fig. 4, a white foamy powder with blue and red parts upon a 254nm excitation was obtained for the two molar ratio (f/o) employed. The best blue/red ratio corresponds to the sample synthesized with the $3(f/o)_{th}$ molar ratio, for which the blue part is more important.

All the characterizations presented in this section have been performed on the powder emitting in the blue range. Characterizations concerning the red part have been published elsewhere (Pradal et al. 2011).

4.1 Structural properties

BAM:Eu^{2+} crystallization was analyzed by means of XRD. Results achieved for the two fuel to oxidizer molar ratios are presented: the stoichiometric molar ratio $(f/o)_{th}$ = 2.36/1 and a fuel-rich one $3(f/o)_{th}$ = 7.08/1.

Fig. 17 shows the XRD patterns of blue phosphors for the two studied molar ratios. Both blue parts correspond to nearly pure $BaMgAl_{10}O_{17}$ phase with a very little fraction of $BaAl_2O_4$, more important for the $(f/o)_{th}$ molar ratio. Since there is a $BaAl_2O_4$ impurity, we have decided to realize an acid-wash. Only washing on the blue powder for the $3(f/o)_{th}$ molar ratio is presented here. Resulting patterns obtained before (Fig. 18a) and after (Fig. 18b) acid-wash are shown in Fig. 18. The experimental XRD pattern after acid-wash reveals that all the diffraction peaks are assigned to the BAM structure. XRD figures also presents the simulated XRD pattern for BAM:Eu^{2+} plotted from the crystallographic data (Kim et al. 2002).

FT-IR spectra of $BaMgAl_{10}O_{17}$:Eu^{2+} blue phosphors for the two studied molar ratios before acid-wash are presented in Fig. 19. Acid-washing does not affect the IR results. Bands ranging from 1000 to 400 cm^{-1} arise from the metal-oxygen (M-O) groups. No band appeared over 1000 cm^{-1}.
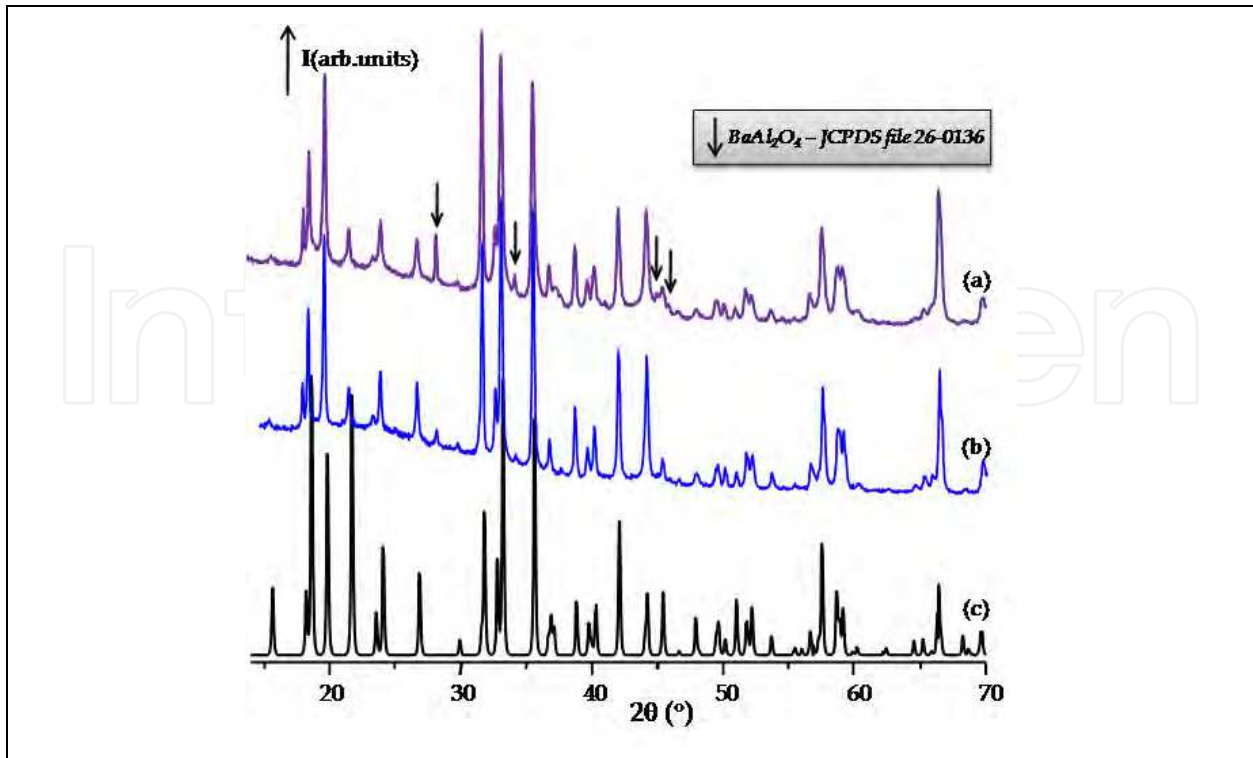
Fig. 17. XRD patterns of blue parts for (a) $(f/o)_{th}$, (b) $3(f/o)_{th}$ and (c) the simulated XRD pattern for BAM:Eu^{2+}.
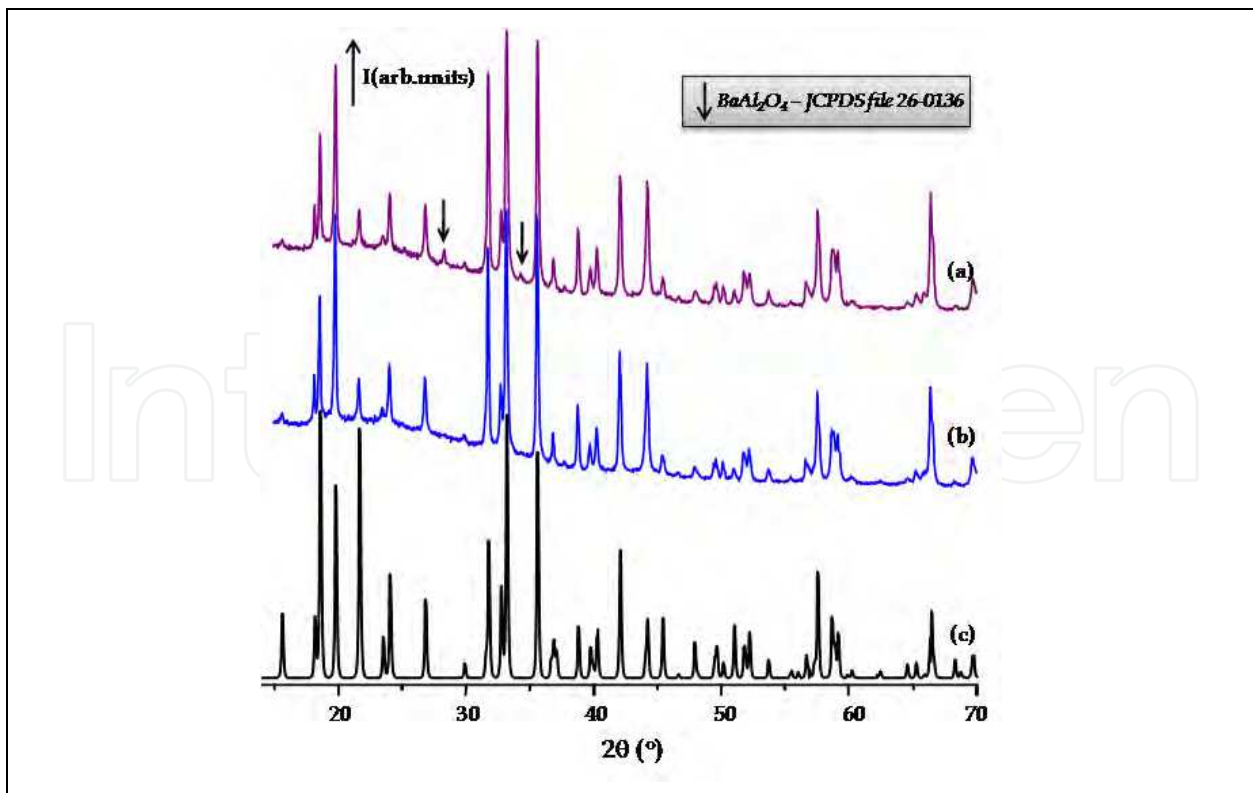

Fig. 18. XRD patterns of blue powder for $3(f/o)_{th}$ (a) before, (b) after acid-wash and (c) the simulated XRD pattern for BAM:Eu^{2+}.
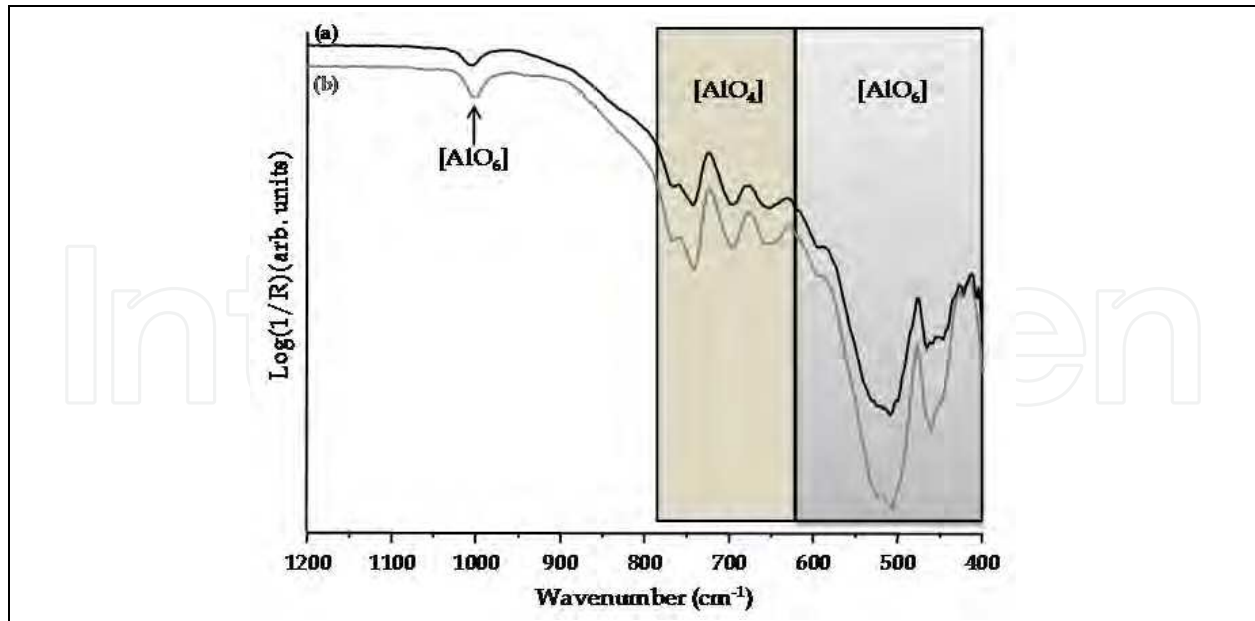
Fig. 19. FT-IR spectra of blue parts for (a) $(f/o)_{th}$, and (b) $3(f/o)_{th}$ before acid-wash.

BAM:Eu^{2+} has a β-alumina structure and belongs to the $P6_3/mmc$ space group. This structure consists of a spinel block composed of aluminium, magnesium and oxygen ($MgAl_{10}O_{16}$) organized in AlO_4 tetrahedrons and AlO_6 octahedrons, so there are two sites for Al^{3+} ions. Mg^{2+} ions occupy one Al site. Two spinel layers are connected by a conduction layer (BaO) where Ba^{2+} ions are substituted by Eu^{2+} (Liu et al. 2009).

Peaks located at 1000 cm^{-1} and from 595 to 445 cm^{-1} are attributed to the absorption of $[AlO_6]$ octahedrons. The absorption peaks, located from 765 to 650 cm^{-1}, can be ascribed to $[AlO_4]$ tetrahedrons (Tian et al. 2006; Zhang et al. 2002).

4.2 Morphological properties

Figs. 20 and 21 show SEM images of blue powders for the two molar ratios studied. For both blue powders, they show a very porous opened microstructure (Figs. 20a and 21a). As for the YAG matrix, this porosity can be correlated with the exothermic character of the combustion and especially with the emission of a large amount of gases during the process. For the theoretical molar ratio $(f/o)_{th}$ (Fig. 20), the particles exhibit two morphologies: rods
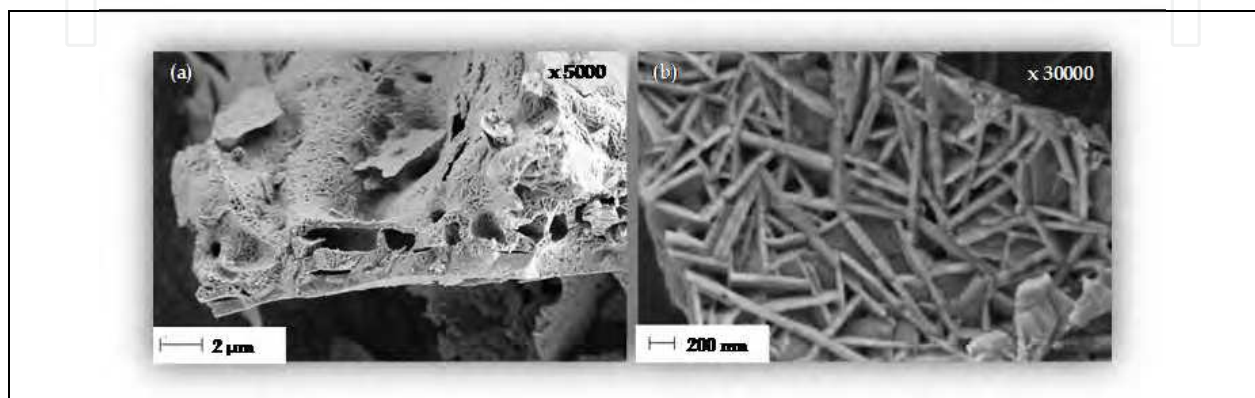

Fig. 20. SEM images of blue powder for $(f/o)_{th}$ (a) x 5000 and (b) x 30000.

and platelets. The width of individual rods lies from 30 to 80 nm whereas their length is contained between 400 and 700 nm. When $(f/o)_{th}$ is increased by a factor of three (Fig. 21), the particles have only a plate-like shape. The platelets thickness varies from 40 to 80 nm and their diagonal from 200 to 500 nm.
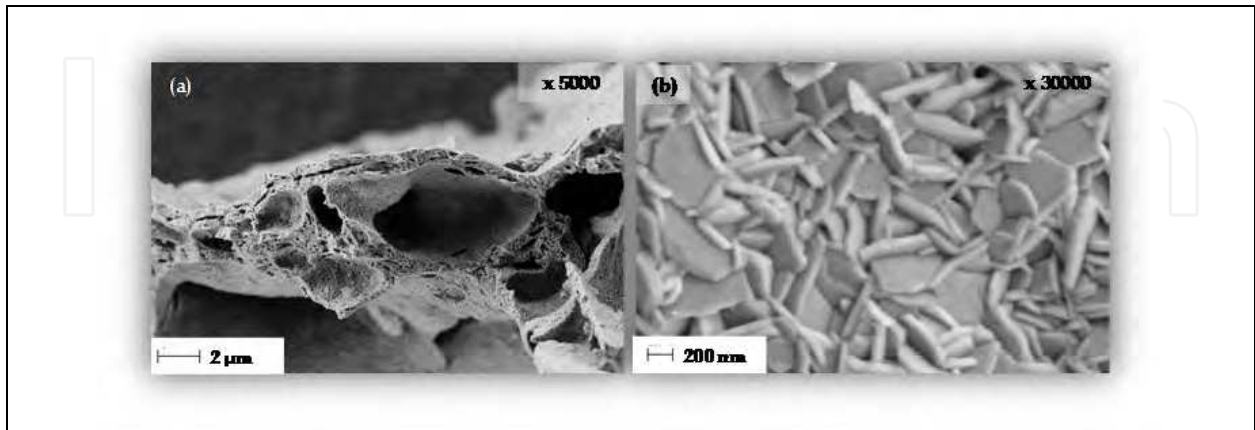

Fig. 21. SEM images of blue powder for $3(f/o)_{th}$ (a) x 5000 and (b) x 30000.

For this ratio, this specific morphology is confirmed with TEM image shown in Fig. 22. Once again acid-washing does not affect the morphological properties.
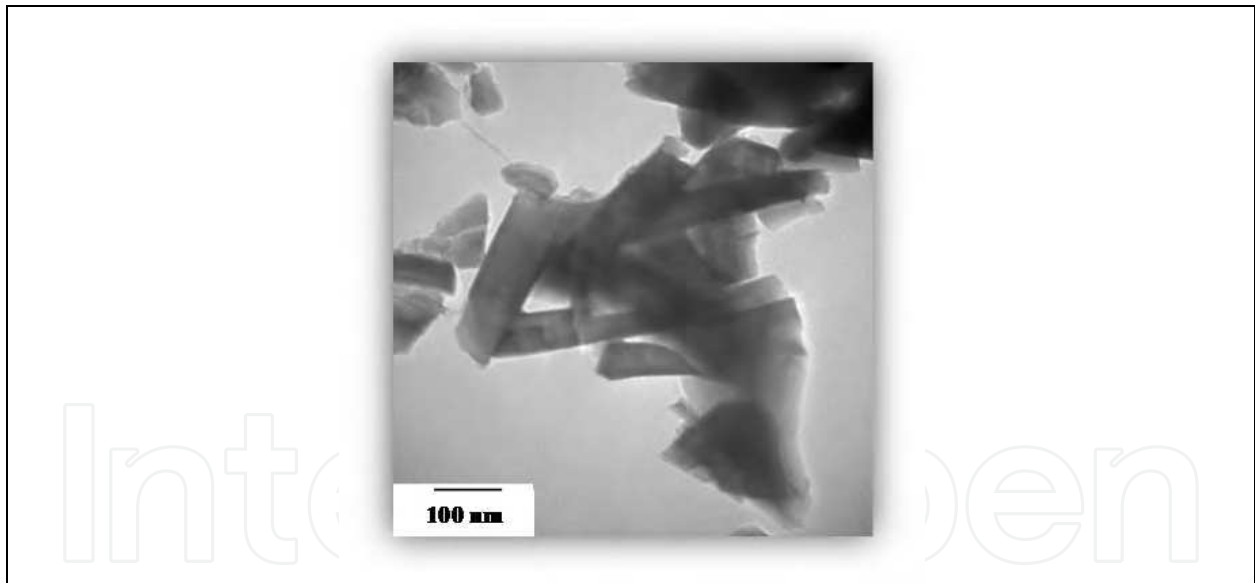

Fig. 22. TEM image of blue powder for $3(f/o)$.

Conventionally, BAM:Eu^{2+} phosphor is obtained via an energy greedy solid-state reaction process requiring a several hour-heating treatment at high temperatures (above 1300 °C). It leads to large size and irregular shapes, inappropriate for the devices foreseen.

SEM image of a commercial BAM:Eu^{2+} powder is shown in Fig. 23. As seen, it presents large and heterogeneous grains. It is very different from powders prepared by a MISCS which are nanostructured and homogeneous. This specific feature, associated with a high crystallinity has several consequences on both the optical performances of this phosphor (see Table 2)

and the capacity for these particles of being dispersed in an aqueous solution to elaborate films. Indeed, particles with a very dense and large size distribution cannot be well-dispersed in a medium and hence cannot be shaped as coatings.
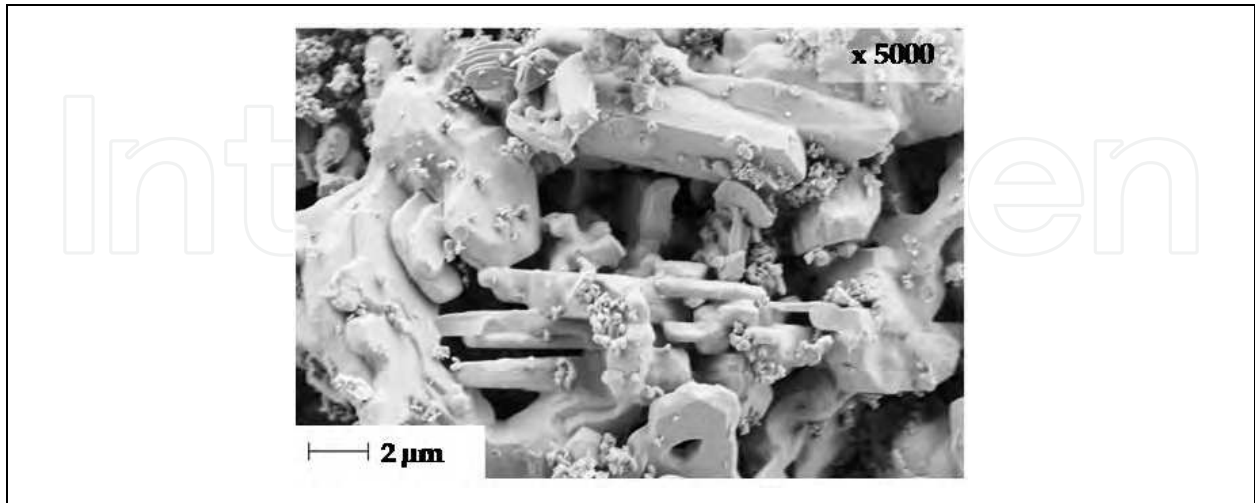

Fig. 23. SEM image of a commercial BAM:Eu^{2+} powder (Rhône Poulenc CRT013).

4.3 Optical properties

Fig. 24 shows emission spectrum of the blue powder for $3(f/o)_{th}$ after acid-wash upon a 382 nm excitation. It consists of a wide band centred at 466 nm. This broad band located in the blue region is due to Eu^{2+} ions transitions from the 4f^{6}5d first excited configuration state to the $^8S_{7/2}$ 4f^7 ground state (Chen & Yan 2007).
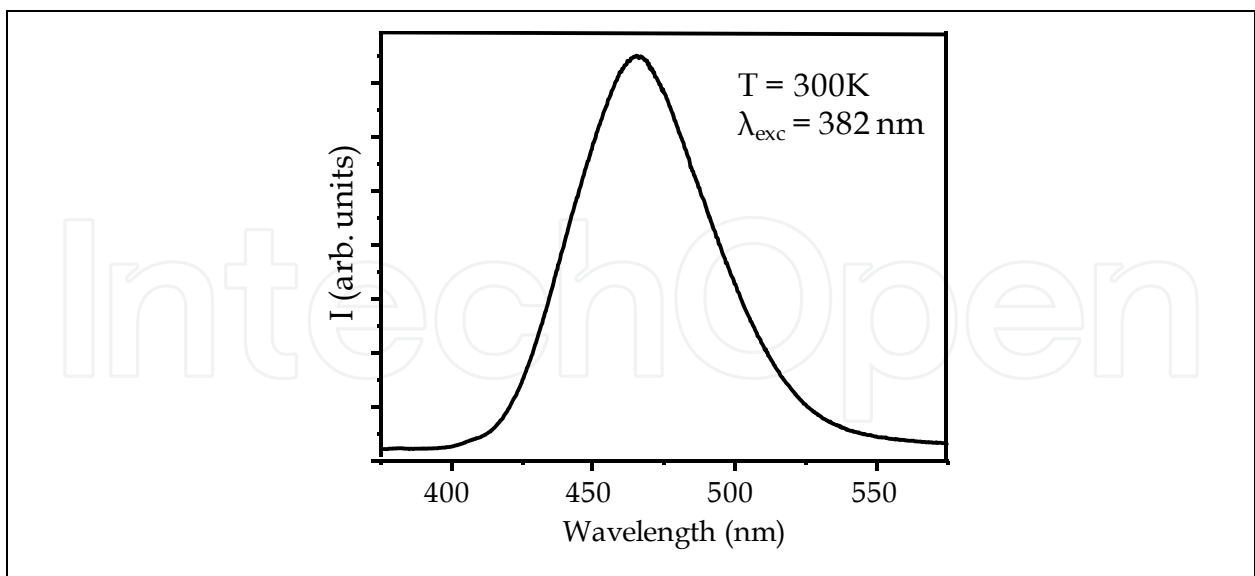

Fig. 24. Room-temperature emission spectrum of blue powder for $3(f/o)_{th}$ upon 382 nm excitation.

The associated excitation spectrum recorded by monitoring the blue emission at 466 nm is shown in Fig. 25. It displays a wide band centred around 382 nm. This absorption band

corresponds to the characteristic Eu^{2+} electronic transition from the ground state to the crystal field split 5d levels (Chen & Yan 2007). This broad excitation band allows considering the combination of BAM:Eu with commercial near-UV LED emitting at 365 nm together with red and green phosphors, in order to produce white light (Smet et al. 2011).
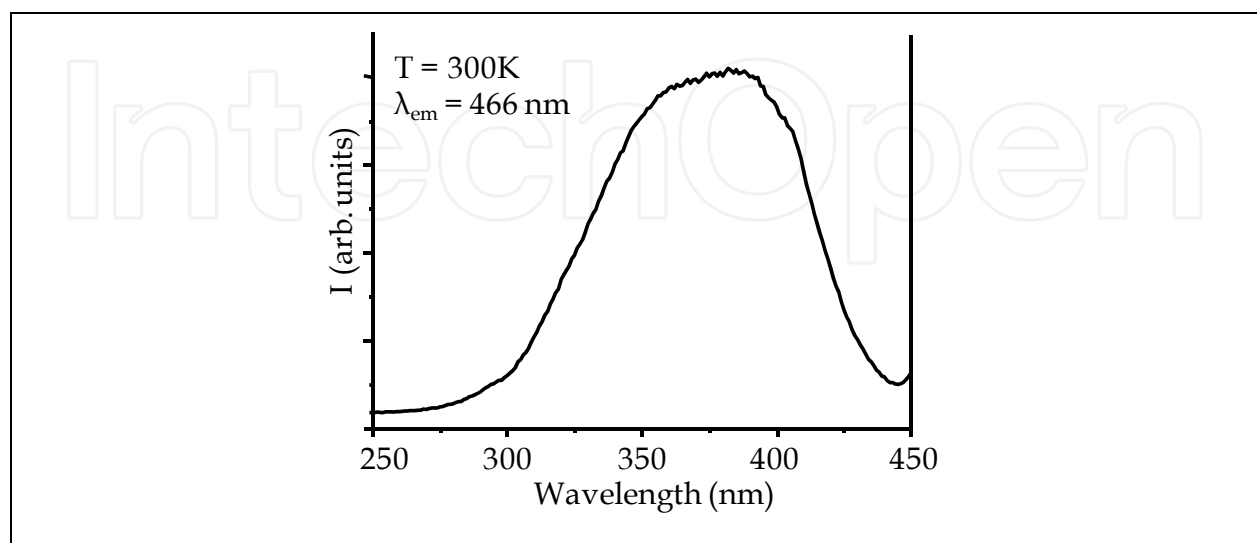

Fig. 25. Room-temperature excitation spectrum of blue powder for $3(f/o)_{th}$ with the emission monitoring at 466 nm.

Finally, photoluminescence quantum yields (in the range 400-650nm) and trichromatic coordinates were recorded by exciting the samples at 365nm, using the equipment detailed in the experimental section. Results are summarized in Table 2.

	QY(%)	x	y
Commercial	88	0.146	0.228
Before washing	79	0.149	0.066
After washing	75	0.149	0.064

Table 2. Absolute quantum yield (QY) and CIE coordinates for commercial BAM:Eu^{2+}powder and MISCS-derived blue powder for $3(f/o)_{th}$ before and after an acid wash, recorded upon a 365 nm excitation.

We can notice that commercial BAM:Eu^{2+} powder presents quantum yield higher than the blue powder resulted from the MISCS for $3(f/o)_{th}$. Furthermore, according to Table 2, acid-washing leads to a decrease of the QY. The main difference between powder before and after acid-wash is that as-prepared powder presents a $BaAl_2O_4$ impurity (see Fig. 18). The presence of $BaAl_2O_4$:Eu^{2+} in our sample does not seem to have a negative effect on BAM:Eu^{2+} luminescence since QY after the acid-wash is worse than that before. Indeed, as it has already been observed (Ravichandran et al. 1999; Singh et al. 2007), MISCS results in the blue shifting of $BaAl_2O_4$:Eu^{2+} emission from 500 nm for a solid-state reaction to about 440 nm. It has to be noticed that the colour coordinates are not modified by washing and that our powders are closer to the ideal blue than the commercial one (see Fig. 26).
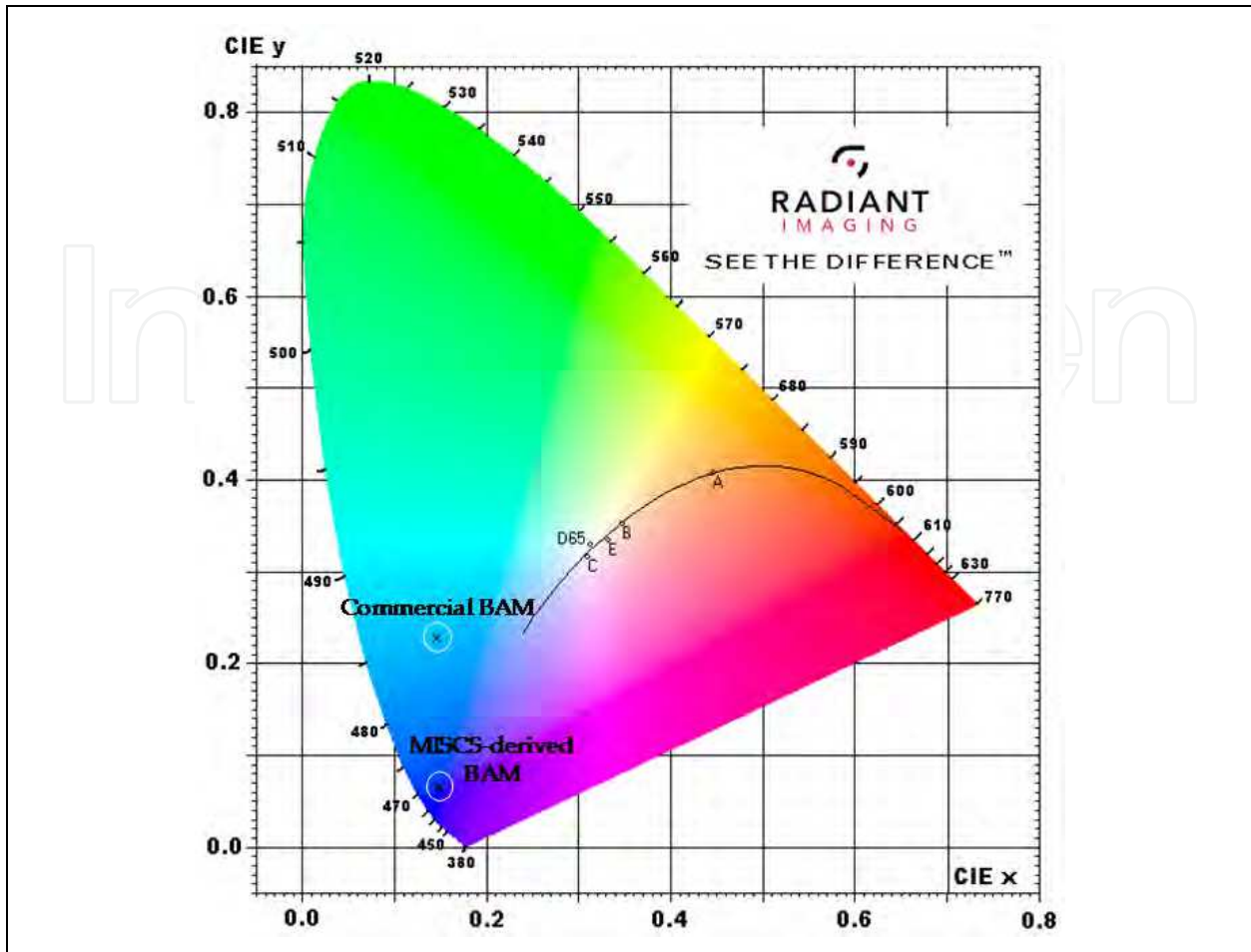
Fig. 26. CIE 1931 colour diagram containing the colour coordinates of BAM:Eu powder synthesized with $3(f/o)_{th}$ before and after an acid wash as well as those of a commercial BAM.

4.4 Shaping of homogeneous films

As mentioned during the study of YAG powders, MISCS-derived phosphors are highly friable and easily grinded into fine particles. These ones can then be homogeneously dispersed into an aqueous or alcoholic solution to give rise to a more or less viscous suspension. This kind of suspension has been used to elaborate a luminescent BAM:Eu film, as shown in Fig. 27.

Fig. 27. Picture of a BAM:Eu^{2+} film under UV excitation.

5. Conclusion

Simple and rapid microwave-assisted combustion procedures have been used to elaborate luminescent YAG:Ce and BAM:Eu powders with suitable quantum efficiencies. The optimal quantity of fuel, leading to the purest aluminates, has been determined to be $3(f/o)_{th}$ in both cases. Furthermore, synthesized powders have revealed to be promising candidates as phosphors for LEDs based lighting devices and can be easily used to make luminescent suspensions, thanks to a uniform and spongious morphology.

Even if the procedures are identical, the features of the powders obtained present significant dissimilarities. For example, as-prepared YAG powders contain carbonaceous impurities, evidenced by their greyish colour, whereas BAM samples do not. As a consequence, YAG:Ce powders need a post-calcination treatment in order to have a respectable quantum efficiency. On the other hand, considering particles morphology, both kinds of samples are very porous and friable but only BAM powders are characterized by a specific nanomorphology (platelets for example). These results can be explained by the fact that microwave radiations absorption depends on the intrinsic properties of ions; hence, the final features of the matrix are closely related to its component and can be tailored by changing the nature of the oxidizers and fuel.

6. Acknowledgment

7. References

Blasse, G. & Grabmaier, B. C. (1994). *Luminescent Materials* Springer-Verlag, ISBN 978-038-7580-19-7, Berlin

Chen, Z. & Yan, Y. (2007). Morphology control and VUV photoluminescence characteristics of $BaMgAl_{10}O_{17}$:Eu^{2+} phosphors. *Physica B: Condensed Matter*, 392, 1-2, pp.1-6, ISSN 0921-4526

Chen, Z., Yan, Y., Liu, J., Yin, Y., Wen, H., Zao, J., Liu, D., Tian, H., Zhang, C. & Li, S. (2009). Microwave induced solution combustion synthesis of nano-sized phosphors. *Journal of Alloys and Compounds*, 473, 1-2, pp.L13-L16, ISSN 0925-8388

Fu, Y.-P. (2006). Preparation of $Y_3Al_5O_{12}$:Ce powders by microwave-induced combustion process and their luminescent properties. *Journal of Alloys and Compounds*, 414, 1-2, pp.181-185, ISSN 0925-8388

Guo, K., Zhang, X.-M., Chen, H.-H., Yang, X.-X., Guo, X. & Zhao, J.-T. (2010). Influence of fuels on the morphology of undoped $Y_3Al_5O_{12}$ and photoluminescence of $Y_3Al_5O_{12}$:Eu^{3+} prepared by a combustion method. *Materials Research Bulletin*, 45, 9, pp.1157-1161, ISSN 0025-5408

Hofmeister, A. M. & Campbell, K. R. (1992). Infrared spectroscopy of yttrium aluminum, yttrium gallium, and yttrium iron garnets. *Journal of Applied Physics*, 72, 2, pp.638-646, ISSN

Höppe, H. A. (2009). Recent Developments in the Field of Inorganic Phosphors. *Angewandte Chemie International Edition*, 48, 20, pp.3572-3582, ISSN 1521-3773

Huang, S. C., Wu, J. K., Hsu, W.-J., Chang, H. H., Hung, H. Y., Lin, C. L., Su, H.-Y., Bagkar, N., Ke, W.-C., Kuo, H. T. & Liu, R.-S. (2009). Particle Size Effect on the Packaging Performance of YAG:Ce Phosphors in White LEDs. *International Journal of Applied Ceramic Technology*, 6, 4, pp.465-469, ISSN 1744-7402

Jain, S. R., Adiga, K. C. & Pai Verneker, V. R. (1981). A new approach to thermochemical calculations of condensed fuel-oxidizer mixtures. *Combustion and Flame*, 40, 0, pp.71-79, ISSN 0010-2180

Jia, D., Wang, Y., Guo, X., Li, K., Zou, Y. K. & Jia, W. (2007). Synthesis and Characterization of YAG:Ce^{3+} LED Nanophosphors. *Journal of the Electrochemical Society*, 154, 1, pp.J1-J4, ISSN 0013-4651

Jung, K. Y. & Kang, Y. C. (2010). Luminescence comparison of YAG:Ce phosphors prepared by microwave heating and precipitation methods. *Physica B: Condensed Matter*, 405, 6, pp.1615-1618, ISSN 0921-4526

Kang, Y. C., Park, S. B., Lenggoro, I. W. & Okuyama, K. (1998). Preparation of non-aggregation YAG-Ce phosphor particles by spray pyrolysis. *Journal of Aerosol Science*, 29, Supplement 2, pp.S911-S912, ISSN 0021-8502

Kim, K.-B., Kim, Y.-I., Chun, H.-G., Cho, T.-Y., Jung, J.-S. & Kang, J.-G. (2002). Structural and Optical Properties of BaMgAl$_{10}$O$_{17}$:Eu^{2+} Phosphor. *Chemistry of Materials*, 14, 12, pp.5045-5052, ISSN 0897-4756

Lee, S. H., Koo, H. Y., Jung, D. S., Yi, J. H. & Kang, Y. C. (2009). Fine-sized BaMgAl$_{10}$O$_{17}$:Eu^{2+} phosphor powders prepared by spray pyrolysis from the spray solution with BaF$_2$ flux. *Ceramics International*, In Press, Corrected Proof, pp.-, ISSN 0272-8842

Liu, B., Wang, Y., Zhou, J., Zhang, F. & Wang, Z. (2009). The reduction of Eu^{3+} to Eu^{2+} in BaMgAl$_{10}$O$_{17}$:Eu and the photoluminescence properties of BaMgAl$_{10}$O$_{17}$:Eu^{2+} phosphor. *Journal of Applied Physics*, 106, 5, pp.053102 - 053102-053105 ISSN 0021-8979

Lu, C.-H., Chen, C.-T. & Bhattacharjee, B. (2006). Sol-Gel Preparation and Luminescence Properties of BaMgAl$_{10}$O$_{17}$:Eu^{2+} Phosphors. *Journal of Rare Earths*, 24, 6, pp.706-711, ISSN 1002-0721

Mangalaraja, R. V., Mouzon, J., Hedström, P., Camurri, C. P., Ananthakumar, S. & Odèn, M. (2009). Microwave assisted combustion synthesis of nanocrystalline yttria and its powder characteristics. *Powder Technology*, 191, 3, pp.309-314, ISSN 0032-5910

Mukasyan, A. S., Epstein, P. & Dinka, P. (2007). Solution combustion synthesis of nanomaterials. *Proceedings of the Combustion Institute*, 31, 2, pp.1789-1795, ISSN 1540-7489

Pan, Y., Wu, M. & Su, Q. (2004). Comparative investigation on synthesis and photoluminescence of YAG:Ce phosphor. *Materials Science and Engineering B*, 106, 3, pp.251-256, ISSN 0921-5107

Potdevin, A., Chadeyron, G., Boyer, D. & Mahiou, R. (2007). Sol-gel based YAG:Ce^{3+} powders for applications in LED devices. *Physica Status Solidi C: Current Topics in Solid State Physics*, 4, 1, pp.65-69, ISSN 1610-1642

Potdevin, A., Chadeyron, G., Briois, V., Leroux, F. & Mahiou, R. (2010). Modifications involved by acetylacetone in properties of sol-gel derived Y$_3$Al$_5$O$_{12}$:Tb^{3+} - II: optical features. *Dalton Transactions*, 39, 37, pp.8718-8724, ISSN 1477-9226

Potdevin, A., Chadeyron, G., Briois, V., Leroux, F., Santilli, C. V., Dubois, M., Boyer, D. & Mahiou, R. (2010). Modifications induced by acetylacetone in properties of sol-gel

derived $Y_3Al_5O_{12}$: Tb^{3+} - I: structural and morphological organizations. *Dalton Transactions*, 39, 37, pp.8706-8717, ISSN 1477-9226

Pradal, N., Potdevin, A., Chadeyron, G. & Mahiou, R. (2011). Structural, morphological and optical investigations on $BaMgAl_{10}O_{17}$:Eu^{2+} elaborated by a microwave induced solution combustion synthesis. *Materials Research Bulletin*, 46, 4, pp.563-568, ISSN 0025-5408

Purwanto, A., Wang, W.-N., Ogi, T., Lenggoro, I. W., Tanabe, E. & Okuyama, K. (2008). High luminance YAG:Ce nanoparticles fabricated from urea added aqueous precursor by flame process. *Journal of Alloys and Compounds*, 463, 1-2, pp.350-357, ISSN 0925-8388

Ravichandran, D., Johnson, S. T., Erdei, S., Roy, R. & White, W. B. (1999). Crystal chemistry and luminescence of the Eu^{2+}-activated alkaline earth aluminate phosphors. *Displays*, 19, 4, pp.197-203, ISSN 0141-9382

Shannon, R. D. (1976). Revised effective ionic-radii and systematic sutdies of interatomic distances in halides and chalcogenides. *Acta Crystallographica, Section A: Foundations of Crystallography*, 32, SEP1, pp.751-767, ISSN 0108-7673

Shen, C., Yang, Y., Jin, S. & Ming, J. (2010). Luminous characteristics and thermal stability of $BaMgAl_{10}O_{17}$:Eu^{2+} phosphor for white light-emitting diodes. *Physica B: Condensed Matter*, 405, 4, pp.1045-1049, ISSN 0921-4526

Shionoya, S. (1998). *Phosphor Handbook* CRC Press, ISBN 978-084-9335-64-8, Boca Raton

Singh, V., Natarajan, V. & Zhu, J.-J. (2007). Studies on Eu doped Ba and Zn aluminate phosphors prepared by combustion synthesis. *Optical Materials*, 29, 11, pp.1447-1451, ISSN 0925-3467

Smet, P. F., Parmentier, A. B. & Poelman, D. (2011). Selecting Conversion Phosphors for White Light-Emitting Diodes. *Journal of the Electrochemical Society*, 158, 6, pp.R37-R54, ISSN

Tian, X., Weidong, Z., Xiangzhong, C., Chunlei, Z., Xiaoming, T. & Xiaowei, H. (2006). Low Temperature Luminescence Properties of Tm^{3+} Doped Aluminate Phosphor. *Journal of Rare Earths*, 24, 1, Supplement 1, pp.141-144, ISSN 1002-0721

Zhang, J., Zhang, Z., Tang, Z., Zheng, Z. & Lin, Y. (2002). Synthesis and characterization of BaMgAl10O17:Eu phosphors derived by sol-gel processing. *Powder Technology*, 126, 2, pp.161-165, ISSN 0032-5910

Zhang, Z., Feng, J. & Huang, Z. (2010). Synthesis and characterization of $BaMgAl_{10}O_{17}$:Eu^{2+} phosphor prepared by homogeneous precipitation. *Particuology*, 8, 5, pp.473-476, ISSN 1674-2001
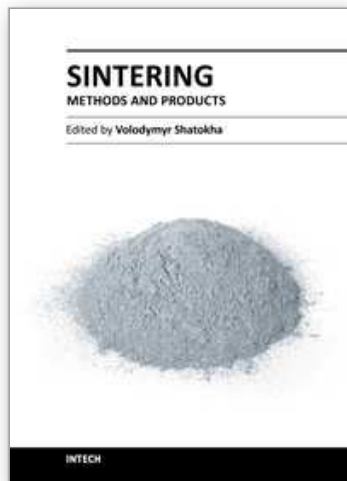
Sintering - Methods and Products

Edited by Dr. Volodymyr Shatokha

This book is addressed to a large and multidisciplinary audience of researchers and students dealing with or interested in sintering. Though commonly known as a method for production of objects from fines or powders, sintering is a very complex physicochemical phenomenon. It is complex because it involves a number of phenomena exhibiting themselves in various heterogeneous material systems, in a wide temperature range, and in different physical states. It is multidisciplinary research area because understanding of sintering requires a broad knowledge - from solid state physics and fluid dynamics to thermodynamics and kinetics of chemical reactions. Finally, sintering is not only a phenomenon. As a material processing method, sintering embraces the wide group of technologies used to obtain such different products as for example iron ore agglomerate and luminescent powders. As a matter of fact, this publication is a rare opportunity to connect the researchers involved in different domains of sintering in a single book.

How to reference

In order to correctly reference this scholarly work, feel free to copy and paste the following:

A. Potdevin, N. Pradal, M.-L. François, G. Chadeyron, D. Boyer and R. Mahiou (2012). Microwave-Induced Combustion Synthesis of Luminescent Aluminate Powders, Sintering - Methods and Products, Dr. Volodymyr Shatokha (Ed.), ISBN: 978-953-51-0371-4, InTech, Available from: http://www.intechopen.com/books/sintering-methods-and-products/microwave-induced-combustion-synthesis-of-luminescent-aluminate-powders

INTECH
open science | open minds